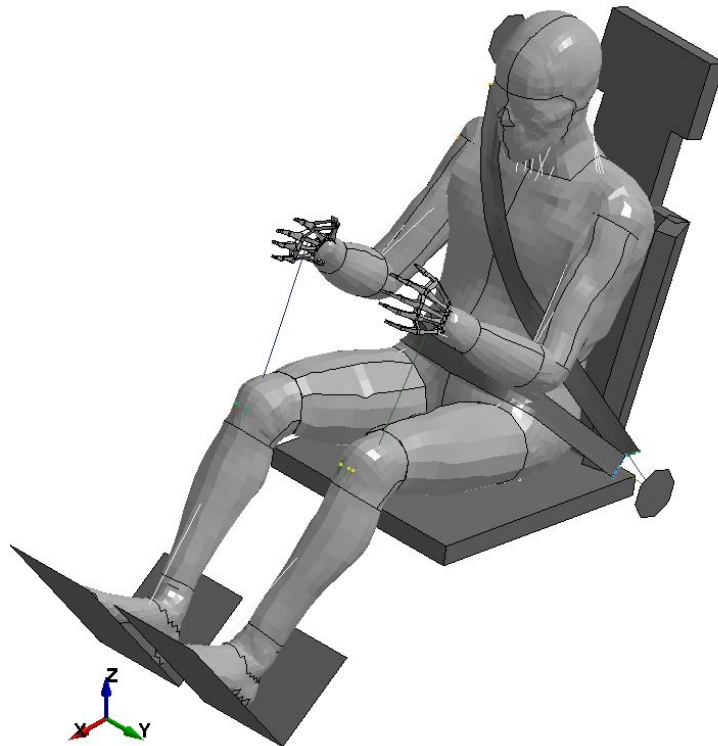




CHALMERS
UNIVERSITY OF TECHNOLOGY



Biofidelity assessment of the active human body model compared to volunteer braking and steering maneuvers

Master's thesis in Applied Mechanics

YANG XIAO

MASTER'S THESIS 2017:86

**Biofidelity assessment of the active human body
model compared to volunteer braking and
steering maneuvers**

YANG XIAO



CHALMERS
UNIVERSITY OF TECHNOLOGY

Department of Applied Mechanics
Division of Vehicle Safety
CHALMERS UNIVERSITY OF TECHNOLOGY
Göteborg, Sweden 2017

Biofidelity assessment of the active human body model compared to volunteer braking and steering maneuvers
YANG XIAO

© YANG XIAO, 2017

Examiner: Karin Brodin, Department of Applied Mechanics

Master's Thesis 2017:86
ISSN 1652-8557
Department of Applied Mechanics
Division of Vehicle Safety
Chalmers University of Technology
SE-412 96 Göteborg
Sweden
Telephone +46 (0)31-772 1000

Cover: SAFER A-HBM in modeled car interior.

Typeset in L^AT_EX
Printed by Chalmers Reproservice
Göteborg, Sweden 2017

Biofidelity assessment of the active human body model compared to volunteer braking and steering maneuvers

YANG XIAO

Department of Applied Mechanics
Chalmers University of Technology

Abstract

Active human body models have contributed to the safety device design and helped build a safer road. Validation is essential for the development of all human models and SAFER A-HBM is no exception. The validation of SAFER A-HBM in multidirection would contribute to the further development of it. Recent research on human body behaviors has been focusing on the frontal and lateral loading direction. But few research looks into the oblique direction. The recently developed SAFER A-HBM is able to work in the omnidirection and needs to validate its effectiveness with the experiment data. By repeating in-vehicle volunteer tests in simulations, which involves oblique maneuvers, visual inspection and correlation analysis have been made between SAFER A-HBM and volunteers. Different setups, such as passive SAFER A-HBM, a different seat and without foot support, are also investigated. Implementing of omni-directional muscles in SAFER A-HBM improves the prediction of head kinematics in pre-crash phase, compared to the model without active muscle. However, the muscle response in lateral direction is still needed to be tuned compared to volunteer response.

Keywords: SAFER A-HBM, Oblique Maneuvers, Biofidelity, Omni-directional

Preface

This work was done as Master thesis at the Division of Vehicle Safety and conducted in the environment of the SAFER Vehicle and Traffic Safety Centre at Chalmers. The simulations were performed on resources at Chalmers Centre for Computational Science and Engineering (C3SE) provided by the Swedish National Infrastructure for Computing (SNIC). Kompetenzzentrum - Das virtuelle Fahrzeug, Forschungsgesellschaft mbH (Graz, Austria) is acknowledged for providing the experimental data in Huber et al. (2015).

Since I am interested in human medical care and health, the thesis work combines those interests and my Master program background. Also my interest in this area has developed since I witnessed the crash test of impact attenuator and learned the importance of vehicle safety in Chalmers Formula Student.

I would like to express my very great appreciation to Professor Karin Brodin for her valuable and constructive suggestions throughout this project. Her generous willingness to give her time is very much appreciated. I would like to offer my special thanks to Dr. Johan Iraeus for his expert assistance, which has been a great help in this project. Many thanks to Robert Thomson for his supervision during the presentation period.

I am deeply grateful to my colleague Jóna Marín Ólafsdóttir for providing me the numerical model, which is used throughout the project. Assistance provided by Christian Kleinbach from University of Stuttgart was greatly appreciated in this project. You are very supportive of me, always willing to help me. Thanks to Andrea Ivancic and Vikram Pradhan for their friendship in the SAFER.

Finally, I wish to acknowledge the understanding and encouragement of my girlfriend and parents throughout my thesis study.

Yang Xiao, Göteborg, October 2017

Terminology and Abbreviations

CNS - Central Nervous System

COG - Center of Gravity

EMG - Electromyogram

FE - Finite Element

HBM - Human Body Model

kph - Kilometres Per Hour

MB - Multibody

MLF - Muscle Length Feedback

NRF - Neck Link Rotation Feedback

PID - Proportional, Integrative and Derivative control

SAFER A-HBM - A human body model with actively controlled muscles previously developed and described in Chapter 3.1.

1D - One Dimensional

3D - Three Dimensional

Contents

List of Figures	xiii
List of Tables	xv
1 Introduction	1
1.1 Vehicle Safety	1
1.2 Numerical HBMs and Volunteer Tests	2
1.3 Aim	4
1.4 Synopsis of Methods	4
2 Background	5
2.1 Volunteer Tests	5
2.2 Biomechanics of Skeletal Muscle	6
3 Methods	9
3.1 The SAFER A-HBM	9
3.2 Experimental Data	10
3.3 Interior Model	11
3.3.1 Seat	11
3.3.2 Seat Belt	13
3.3.3 Foot Support	15
3.3.4 Positioning	15
3.3.5 Load Case	15
3.4 Output Parameters	18
3.5 Biofidelity Score Calculation - CORA	18
3.6 Simulation Summary	19
4 Results	21
4.1 Kinematic Comparisons of SAFER A-HBM	21
4.1.1 Brake Event	21
4.1.2 Lane Change Right Event	24
4.1.3 Combined Change Right Event	25
4.2 Modification of Muscle Activation and Interior Model	26
4.2.1 Brake Event	27
4.2.2 Lane Right Event	29
4.2.3 Combined Right Event	30
4.3 Biofidelity Score - CORA	31

5 Discussion	33
6 Conclusion	35
Bibliography	37
References	37
A Code	I
A.1 Plot Kinematics with Corridor in MatLab	I
A.2 Output Node Macro in LS-PrePost	XIV
B Load Scenarios	XVII

List of Figures

2.1	Hill model	7
3.1	Seat dimensions in experiment without side support, from Kirschbichler et al. (2014)	10
3.2	Vehicle and volunteer during experiment from Huber et al. (2015) . .	11
3.3	Modeled interior in isometric view	12
3.4	Modeled interior in xz plane	12
3.5	Modeled seat in isometric view	12
3.6	Shoulder seat belt and lap seat belt with line elements and spring elements at two ends	13
3.7	Seat in experiment from Huber et al. (2015)	13
3.8	Three spring stiffness at 0 mm, 40 mm and 80 mm offsets	14
3.9	Torso displacement Δr_x^{torso} for three spring stiffness	14
3.10	Torso center displacement in x axis at global damping factors 0 and 0.15	16
3.11	The SAFER A-HBM in the interior, indicating the coordinate system	17
3.12	User defined corridor. Read line was comparison curve. Green lines formed inner corridor. Blue lines formed the outer corridor.	19
3.13	Default CORA corridor. Read line was comparison curve. Green lines formed inner corridor. Blue lines formed the outer corridor.	19
4.1	Torso displacement Δr_x^{Torso}	21
4.2	Head displacement Δr_x^{Head}	21
4.3	Torso angle change Φ_y^{Torso}	22
4.4	Torso bending angle $-\Phi_y^{Torso} - \phi_y^{Torso}$ of SAFER A-HBM in brake event.	22
4.5	Torso rotation angle ϕ_z^{Torso} of SAFER A-HBM in brake event.	22
4.6	Head rotation angle ϕ_z^{Head} of SAFER A-HBM in brake event.	22
4.7	Shoulder belt force of SAFER A-HBM in brake event.	23
4.8	Lap belt force of SAFER A-HBM in brake event.	23
4.9	Torso displacement Δr_y^{Torso} of SAFER A-HBM in lane right event. . .	24
4.10	Head displacement Δr_y^{Head} of SAFER A-HBM in lane right event. . .	24
4.11	Torso angle change Φ_x^{Torso} of SAFER A-HBM in lane right event. . .	24
4.12	Torso bending angle $-\Phi_x^{Torso} - \phi_x^{Torso}$ of SAFER A-HBM in lane right event.	24
4.13	Torso displacement Δr_x^{Torso} of SAFER A-HBM in combined right event.	25
4.14	Head displacement Δr_x^{Head} of SAFER A-HBM in combined right event.	25
4.15	Torso displacement Δr_y^{Torso} of SAFER A-HBM in combined right event.	26

4.16	Head displacement Δr_y^{Head} of SAFER A-HBM in combined right event.	26
4.17	Comparison of torso displacement Δr_x^{Torso} during brake event in setups SAFER A-HBM, passive SAFER A-HBM, Taurus seat and without foot support.	27
4.18	Comparison of head displacement Δr_x^{Head} during brake event in setups SAFER A-HBM, passive SAFER A-HBM, Taurus seat and without foot support.	27
4.19	Comparison of torso angle change Φ_y^{Torso} during brake event in setups SAFER A-HBM, passive SAFER A-HBM, Taurus seat and without foot support.	28
4.20	Comparison of torso bending angle $-\Phi_y^{Torso} - \phi_y^{Torso}$ during brake event in setups SAFER A-HBM, passive SAFER A-HBM, Taurus seat and without foot support.	28
4.21	Comparison of torso rotation angle ϕ_z^{Torso} during brake event in setups SAFER A-HBM, passive SAFER A-HBM, Taurus seat and without foot support.	28
4.22	Comparison of head rotation angle ϕ_z^{Head} during brake event in setups SAFER A-HBM, passive SAFER A-HBM, Taurus seat and without foot support.	28
4.23	Comparison of torso displacement Δr_y^{Torso} during lane right event in setups SAFER A-HBM, passive SAFER A-HBM and Taurus seat.	29
4.24	Comparison of head displacement Δr_y^{Head} during lane right event in setups SAFER A-HBM, passive SAFER A-HBM and Taurus seat.	29
4.25	Body motion on Taurus seat when the maximum y displacement occurred.	29
4.26	Body motion on testing seat when the maximum y displacement occurred.	29
4.27	Comparison of torso angle change Φ_x^{Torso} during lane right event in setups SAFER A-HBM, passive SAFER A-HBM and Taurus seat.	30
4.28	Comparison of torso bending angle $-\Phi_x^{Torso} - \phi_x^{Torso}$ during lane right event in setups SAFER A-HBM, passive SAFER A-HBM and Taurus seat.	30
4.29	Comparison of torso displacement Δr_x^{Torso} during combined right event in setups SAFER A-HBM, passive SAFER A-HBM and Taurus seat.	31
4.30	Comparison of head displacement Δr_x^{Head} during combined right event in setups SAFER A-HBM, passive SAFER A-HBM and Taurus seat.	31
4.31	Comparison of torso displacement Δr_y^{Torso} during combined right event in setups SAFER A-HBM, passive SAFER A-HBM and Taurus seat.	32
4.32	Comparison of head displacement Δr_y^{Head} during combined right event in setups SAFER A-HBM, passive SAFER A-HBM and Taurus seat.	32
B.1	Load Case Brake. Data is from Huber et al. (2015)	XVII
B.2	Load Case Lane Change Right. Data is from Huber et al. (2015)	XVII
B.3	Load Case Combined Change Right. Data is from Huber et al. (2015)	XVII

List of Tables

3.1	Prescribed direction for three maneuvers	17
3.2	Node number for calculating kinematic parameters	18
3.3	Simulations matrix	20
4.1	Summary of qualitative assessment	21
4.2	Summary of the parameters	27
4.3	CORA rating of brake event	31

1

Introduction

1.1 Vehicle Safety

Vehicle safety devices play critical roles in reduction of road mortality. After introduction of compulsory usage of three-point belt by Swedish belt use law in 1975, the injury rate had reduced 19% in the following year (Norin et al., 1984). The Electronic Stability Control (ESC) had a minimum of 35% the effectiveness of the reduction in fatal crashes on slippery roads during 1998 to 2004 (Lie et al., 2006). Even though, there were 319 fatalities in Sweden (Energy, 2012) in 2012, 31 000 fatalities in 27 EU countries (Energy, 2012) in 2012, and 35 092 fatalities in the USA (Administration et al., 2016) in the year 2015. In order to further reduce the road injures and deaths, European Commission set a goal of reducing the number of injuries and deaths to half of the number during 2001-2010 by 2020 and to almost 0 by 2050 (Commission et al., 2011). That highlights the need for safer vehicles. Injuries during low-speed collision, like potential whiplash injury and bone fracture of the rib cage have also attracted researchers' attention (Penning, 1992; Magnusson et al., 1999).

The last few decades have witnessed a growing trend towards the utilization of various methods to promote vehicle safety, e.g. more advanced occupant restraint system, volunteer test, the anthropomorphic test device (ATD), cadaver test, animal test, human body model (HBM).

The ATD is also known as a crash test dummy, which is mechanical models of a human body during physical test. They are valuable tools to evaluate the new vehicle design regarding the protection potential of different restraint systems in simulated collisions.

During low-speed frontal collision, human volunteers and ATD would perform differently in biomechanical responses, for example, volunteers instructed to brace their arms would have quite different kinematics to ATD (Beeman et al., 2012).

Scott et al. (1993)'s work has shown a difference in in head kinematics between ATD and human during low-speed rear impact. Östh and Olafsdottir's work has shown that both female and male volunteer drivers have considerable activities in cervical and lumbar extensors, as well as shoulder and elbow extensors during braking (Östh et al., 2013). That muscle-induced movement plays an important role in brake event. A precise prediction of the occupant response would help investigate the possibility of interactions between car interior and human head motion, which help to improve the safety devices. So simulation or testing should involve active muscles in order to predict injuries better.

The issue of active HBM has received considerable attention. Recent evidence from different studies suggests that the active HBM gives a good prediction for some load scenarios. Östmann and Jakobsson (2016) shows that the active HBM is a feasible tool to duplicate occupant performance from pre-crash phase to crash phase, improving the evaluation of safety devices. The work done by Östh (2014) and Ólafsdóttir (2017) contributed to the development of SAFER A-HBM. Östh's work developed the active muscles for sagittal plane motion. Olafsdottir's work developed a model which was capable of simulating omnidirectional head kinematics.

This study offers some important insights into the biofidelity assessment of the omnidirectional SAFER A-HBM by comparing simulation results with experimental data.

1.2 Numerical HBMs and Volunteer Tests

In 1963, McHenry (1963) developed a nonlinear mathematical model of a human body to study the dynamic response of the occupant and the restraint system, which was one of the very first research into that. Over the past few decades, there has been a dramatic increase in the computational ability. More and more complex numerical HBMs have been developed and used for predicting occupant movement during the crash phase, saving time and money in the automotive industry, achieving similar results as physical testing (Prasad & Chou, 2002). Two main approaches represent numerical human body models. One is the multi-body (MB) model, the other one is the finite element (FE) model.

The MB model assumes the occupant to be a set of flexible and rigid bodies, endowed prescribed masses and moments of inertia, connected by kinematic joints. It has an advantage in requiring less computing capabilities. Three well-accepted models in the automotive industry are CAL3D, MVMA2D and MADYM02D/3D (Prasad & Chou, 1993). There are also models for specialized usage, like DOT-SID model for side impact simulations, program SOMLA for combining a MB model with a FE seat model.

The FE model approximates occupant by dividing the anatomical structure into many small elements, where partial differential equations are applied, generating approximated values of the unknowns over the anatomical structural domain at certain discrete points. It requires more computational resources than MB model but could predict more details, like injuries at tissue levels. In 1975, one FE model was promoted by Schugar for the development of head injury model (Shugar & Katona, 1975). In the early phase of the development of FE model, the research focused on specific parts of the human body (Yang et al., 2006).

Due to advances in the computational abilities in recent decades, whole body FE HBMs come into view, e.g. HUMOS in 2001 (Robin, 2001), THUMS in 2002 (Iwamoto et al., 2002), GHBM in 2013 (Park et al., 2013). In 1987, Deng and Goldsmith (1987) had first tried to implement the MB with muscle properties for head, neck and upper-torso, even though the numerical model showed some difference compared to testing. For some models, the passive properties of the muscles are included, e.g. Jost and Nurick (2000) (Visco-elastic properties were simplified with elastic behavior and damper elements were added), Robin (2001), Ejima et al.

(2005) (They suggest that a model with solid passive elements is consistent with the relaxed impact condition).

Extensive studies have been put on active muscle properties recently, which means the forces generated by muscles are taken into consideration for the numerical model. One of the well-known models in MB models is TNO Active Human Model. It has been continuously developed since 2008 by Meijer, Rodarius, Adamec, van Nunen, and Van Rooij (2008), Nemirovsky and Van Rooij (2010), Meijer et al. (2012), implementing open loop and closed loop, proportional, integrative and derivative (PID) controllers for cervical spine and whole body.

Several researchers have also implemented the active muscle on the FE models. Brolin et al. (2005) investigate active neck muscle properties of cervical spine in a FE model developed by Brolin (2002) and Halldin (2001). Actuator is modeled with 1 D Hill type muscle model, with optimal muscle length and peak force predefined. Active muscles used open loop control with 6 predefined activation curves. Frontal and lateral volunteer tests are conducted to validate the model. It is found that the model correlates with the experimental data best at a certain percentage muscle activation and the activation of muscles in cervical spine would contribute to decrease ligament injury risk for both frontal and lateral impact.

Choi et al. (2005) in solver PAM-CRASH for upper and lower extremities, Behr et al. (2006) in solver Radioss for lower extremities, Brolin et al. (2008) in FE code LS-Dyna for cervical spine, Östh (2014) for the whole body in sagittal plane, and Ólafsdóttir (2017) for multidirectional head and neck response.

Iwamoto et al. (2011) have developed 3 D geometry muscles for numerical body to investigate effects of bracing during pre-crash phase. The passive muscles are modeled with solid elements while the active muscles are modeled with Hill type bar elements (without passive parts). Brake test has been conducted to find the muscle activities of braced arms in pre-impacts in a laboratory. Activation level was determined based on the EMG test data from the volunteer testing. Frontal impact simulations at speed 50 kph show that the active HBM appears to be less risky to suffer from rib fracture than the cadaveric HBM.

Volunteer tests at low impact loads have been continuously conducted for gaining knowledge of occupant response and muscle activation. The volunteer experiments have been set up either on sled (Arbogast et al., 2009), or in vehicle under test/real track environment (Carlsson & Davidsson, 2011), or on simulator (Hault-Dubrulle et al., 2011). Many of the experiments focus on loading in longitudinal and lateral direction, e.g. Stockman et al. (2013)'s research is doing brake and steering events in a vehicle for the child volunteers, Ejima et al. (2012) have done an experiment at low-speed lateral load on a sled. One oblique load testing was done by Shaw, Herriott, McFadden, Donnelly, and Bolte IV (2006) for ATD, which was common in oblique loading instead of human volunteers. Arbogast et al. (2012) have done the oblique loading for the human volunteers. on the sled. Huber et al. (2015)'s work is one of the very first to implement oblique direction load in vehicle test for volunteers.

Volunteer test in a vehicle could provide data sets for validating the human body model. Östh et al. (2013) involved 20 volunteers as both drivers and passengers on a closed test track. Body kinematic data and surface EMG signals during au-

onomous braking were collected in pre-crash phase, used to validate the SAFER A-HBM. the SAFER A-HBM. Besides, Ólafsdóttir et al. (2015) measured the cervical muscle reflexes in 3 D perturbations, which supported the development of the omni-directional SAFER A-HBM in omnidirectional head kinematic.

1.3 Aim

This study evaluates the biofidelity of the omni-directional SAFER A-HBM for three events; braking, lane change to the right, and combined braking and lane change to the right. Another purpose is to explore affects of different setups, passive SAFER A-HBM, SAFER A-HBM on a Taurus seat, SAFER A-HBM on an interior model without pedal.

1.4 Synopsis of Methods

This study uses both visual inspection and correlation analysis approaches to study the kinematics of the SAFER A-HBM in different condition. By employing a visual inspection, this study attempts to evaluate the performance difference between SAFER A-HBM and the experiment qualitatively. By using the correlation analysis, ratings are given to different models as a quantitative approach.

2

Background

2.1 Volunteer Tests

Three publications from Ejima et al. presented frontal and lateral low-speed sled tests. In 2007, Ejima et al. (2007) did frontal low-level impact sled test with 5 volunteers and concluded that muscle activation level would influence the after impact kinematics considerably. In the next year, Ejima et al. (2008) conducted low-speed front impact sled test to investigate volunteers' physical response, involving 2 female and 5 male volunteers. It concluded that four phases could be divided into after the beginning of the impact and more details were revealed about several major muscle groups, e.g. muscle paravertebralis, muscle obliquus externus abdominis. The muscles were activated at around 130 ms after the onset of impact. A strong correlation was found between the activation of muscle and head-neck-torso movement. In 2012, Ejima et al. (2012) conducted low-speed lateral sled tests to investigate emergency steering maneuvering. Three volunteers were initially instructed to relax and tense their muscles. Neck, abdomen, and back muscles were found to be mainly activated during steering maneuvering. Through a comparison with dynamic response and EMG data, Ejima et al. concluded that relaxed and tensed muscle would influence the body response much, reaching posture control effect 20-40% for lateral flexion muscle group, and indicated that the EMG data was useful for predicting the body motion.

Kemper et al. (2011) performed frontal sled tests with 5 male volunteers in 2011, to investigate the relation between arm bracing and chest compression. It showed that arm bracing helped reduce upper body excursion and chest compression during thoracic belt loading for all 5 subjects. However, 2 subjects had increased sternum depth due to up extremities activities. Beeman et al. (2012) conducted frontal sled tests with 5 male volunteers, one Hybrid III ATD and three male PMHS. It concluded that those three categories showed kinematic differences when volunteers were instructed to be relaxed, and significant differences were found when the volunteers were instructed to be braced.

Researchers van Rooij et al. (2013) did lateral tests on a test vehicle in a laboratory environment with 10 volunteers. Four-point-belt was used for lateral evasive maneuver and 10 subjects were instructed to be relaxed and braced. Corridors of different body parts were created. Larger body motion and higher muscle activation levels were found in braced volunteers than relaxed volunteers on the passenger seat.

In 2011, Carlsson and Davidsson (2011) implemented vehicle based volunteer brake tests involving 8 females and 9 males on an ordinary road to examine maximum

driver brake and autonomous brake (deceleration: $3 - 5 \text{ m/s}^2$). The conclusion was that female showed larger excursion than male and passengers showed larger forward motion than drivers. In 2013, Ólafsdóttir et al. (2013) implemented vehicle-based brake autonomous tests for 20 volunteers with standard three point belt and pre-tension belt. It concluded that all muscle groups were having an obviously higher level of activation and pre-tension belt helped reduce the head and neck forward displacement. Corridor data about EMG and dynamics were presented. In 2013, Östh et al. (2013) did volunteer braking testings involving 11 male and 9 female on an ordinary traffic situation, to investigate kinematics and EMG data. It concluded that muscle activation level increased from less than 10% to 13–44% in the cervical and lumbar muscle group. The pre-tension belt would advance 71-176 ms for the onset of muscle activation. Corresponding kinematic and EMG data were presented. Arbogast et al. (2012) investigated the effect of pretensioned seat belt to people in different age groups under low-severity lateral and oblique impact. 30 male volunteers were involved. electromechanical motorized seat belt retractor (EMSR) data sets and body kinematics like displacement of the torso, angle between the sternum and the shoulder belt were recorded. Tests of different arms' position were also conducted. Writers concluded that effect of pretensioning was strong. The data sets collected during experiments could be used to validate the responses of human body models.

Kirschbichler et al. (2014) did brake and lane change maneuvers in test vehicle with more than 24 volunteers in 2014. They showed inter-individual differences were significant when a lap belt was used. Besides, side support of the seatback would change the kinematics of occupant during the lane change.

Huber et al. (2014) showed a very brief introduction about a vehicle test carried out under oblique loading in 2014, involving 6 female and 27 male volunteers. That paper was followed by Huber et al. (2015) in the year 2015, which provided the experimental data used in this study.

2.2 Biomechanics of Skeletal Muscle

Skeletal muscle, together with heart muscle and smooth muscle, makes up 23% body mass for female and 45% for male (Itskov, 2016). Skeletal muscle contributes to active movements, maintenance of body position, energy conversion and heat production. Its hierarchical composition could be broken down from muscle to fasciculus, a group of muscle fibres, myofibril, myofilaments, and to myosin and actin in the end. The muscle fibers would obey the "all or none" rule, which means that they will always contract to the maximum. Permanent contraction with a constant force of muscle twitching is called tetanized state. The force in a tetanized state muscle is depending on the velocity of the muscle contraction, which is known as Hill curve: $(T + a)(\nu + b) = (T_0 + a)b$, proposed by Hill (1938). Skeletal muscle can be activated due to electric, chemical or nervous stimulation. A physical model (Figure 2.1), Hill's three element model, could describe the interaction between passive elastic and active muscle fibers, by using a parallel element, a contractile element, and a series element (Siebert et al., 2008).

Muscle contraction is controlled by central nervous system (CNS). The muscle fibers

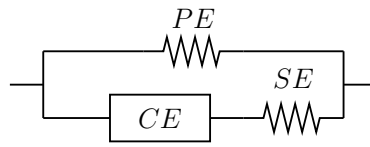


Figure 2.1: Hill model

receive a contraction signal, an action potential is propagated along the muscle fibers. The action potential can be collected experimentally as the electromyogram (EMG). After the action potential, calcium ions are released in the muscle fibers, resulting in muscle tension. Afterwards, the cell membrane is restored and the calcium level is reduced, leading to muscle tension drops. The conduction inside neurons is very fast but between neurons is relatively slow due to chemical synapse. Thus, neural delay is always observed when neural signal is sent to skeletal muscles (Östh, 2014).

2. Background

3

Methods

The active HBM used throughout this study was the omni-directional SAFER A-HBM, described in Section 3.1. Three volunteer experiments (Huber et al., 2015), described in Section 3.2, were simulated and the interior model used is described in Section 3.3. The output taken from the SAFER A-HBM is described in section 3.5 and section 3.6 summarizes all simulations performed.

Commercial FE code, LS-Dyna (version mpp, double precision, R810) (LSTC, Livermore, CA, USA) were used for all simulations to solve the motion equations numerically, in which explicit solver was used based on central difference theorem. All pre- and post-processing in this thesis was done using LS-PREPOST (LSTC Inc., Livermore, CA, USA) and MATLAB (The Mathworks Inc., Natick, MA, USA). Catia V5 (Dassault Systèmes, France) was used to create the 3 D model for the seat.

3.1 The SAFER A-HBM

Total Human Model for Safety (THUMS) is a widely used FE model and is developed by Iwamoto et al. (2002). It is a finite element model of 50th percentile American male occupant. The aim is to study the occupant behaviors during impact scenarios. THUMS has more than 80 000 elements in total and each element has a reasonable size and shape to achieve suitable computer running time. Bones are modeled with isotropic elastic plastic shell and solid elements for cortical parts and spongy part. Skin is modeled with elastic shell elements, while other soft tissues are modeled with a viscoelastic material in solid elements, e.g. flesh and fat, organs. Tension-only elastic material properties are for muscle in bar elements. Each body part has been developed and validated for frontal or side impacts using existing cadaver test publications. An overall model is validated against an accident in the real world. Another validation done by Maeno and Hasegawa (2001) contributes to the validation of whole body kinematics and lower extremity model. Those validation shows good correlation between the THUMS and the actual accidents in injuries criteria, e.g. rib fracture and head injures. THUMS is a tool showing good agreement with experiments in injury.

The omnidirectional SAFER A-HBM used in this project is a beta version (mod 2.5) developed by Ólafsdóttir (2017), which is based on the THUMS version 3.0. Those active muscles were written into 3 keyword files, which were respectively for the lower extremities (version 1.0, date: 2014/02/14), neck and trunk (version 1.0, date: 2014/02/14, omnidirectional controller added), and upper extremities (version 1.0,

date: 2014/02/14). The detailed LS-Dyna solver version is: ls-dyna mpp d R810 winx64 ifort131 pmpi.

Compared to the model developed by Östh (2014), measurement of the posture would be done in three dimensions instead of just sagittal plane (Ólafsdóttir, 2017). The used version of model adopted the neck link rotation feedback(NRF), which means the model only got feedback from the kinematics of the neck link (Spine T1 vertebrae to head COG). Olafsdottir also proposed other methods to measure body posture, such as getting feedback from the length of the muscle(MLF) and a combination of NRF and MLF.

The rotation of the neck link was used as input for backwards closed loop PID control. Angle change of the neck link was measured to know change of body posture and then activation level value was generated from the controller in individual muscle element. Afterwards, muscle material was activated and generated forces to influence the kinematics of the SAFER A-HBM. Muscle activation level in the Hill type muscle elements in the lower and upper extremities was 0.

3.2 Experimental Data

Load scenarios, occupants response data and interior used in this study came from the experiments done by Huber et al. (2015) and only their simulation sets were simulated. The experimental data in Huber et al. (2015) is owned by Kompetenzzentrum - Das virtuelle Fahrzeug, Forschungsgesellschaft mbH (Graz, Austria) and was only processed in this study for the purpose of model validation. Foam, side support and shoulder belt were added to the seat described in Figure 3.1, which was referred for creating the modeled seatpan and seatback. Three types of load maneuvers were conducted: brake, lane change and combined maneuver. In total six females and nineteen males joined the volunteer tests on a closed test track.

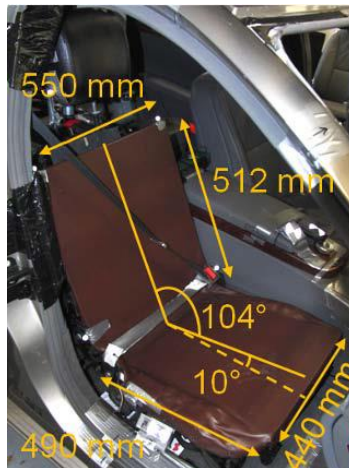


Figure 3.1: Seat dimensions in experiment without side support, from Kirschbichler et al. (2014)

The experiment used a modified Mercedes-Benz S class vehicle, shown in Figure 3.2.

Eight cameras and test suits were used to record the kinematics of the body, illustrated in Figure 3.2. Electronic senses recorded vehicle conditions: vehicle velocity, frontal and lateral acceleration, steering angle and angular velocity, yaw rate and brake pedal activation state. Every load event started at velocity 50 kph. Time $t = 0$ started when brake pedal moved during brake and combined maneuvers. For lane change maneuver, time $t = 0$ was decided based on a extrapolation at 20 deg of angle change of steering wheel.



Figure 3.2: Vehicle and volunteer during experiment from Huber et al. (2015)

Correction algorithm was applied for compensating camera vibrations. Rigid body motion was assumed for the trajectory between markers. Median, 0.16 quantile and 0.84 quantile values of the 25 volunteers' kinematics were calculated to create occupant kinematic corridor. Span between upper boundary and lower boundary corresponded to one standard deviation.

Kirschbichler et al. (2014) investigated several factors that may influence the occupant kinematics. It showed significant differences among individuals in occupant movement. Significant difference between with side support and without side support was found.

3.3 Interior Model

Figure 3.3 (isometric view) and Figure 3.4 (right view) show the modeled interior, containing one seat, two foot supports, seat belts, and three belt attachments. In total 5 690 solid elements, 4 552 shell elements, two discrete elements, three mass elements, and 30 seat belt elements were created. According to the rules for judging mesh quality promoted by Burkhart, Andrews, and Dunning (2013), mesh quality of the interior model was good. 1.4 % solid elements and 0 % shell element had an aspect ratio above 3, which was less than the criteria 5 %. Another rule was that less than 5 % of the elements should have a Jacobian below 0.7, while all shell elements in the interior were above 0.7.

3.3.1 Seat

Seat Geometry: The geometry file of the seat was created in Catia V5. Seatpan and seatback were drawn based on Figure 3.2. Afterwards, two side supports at the

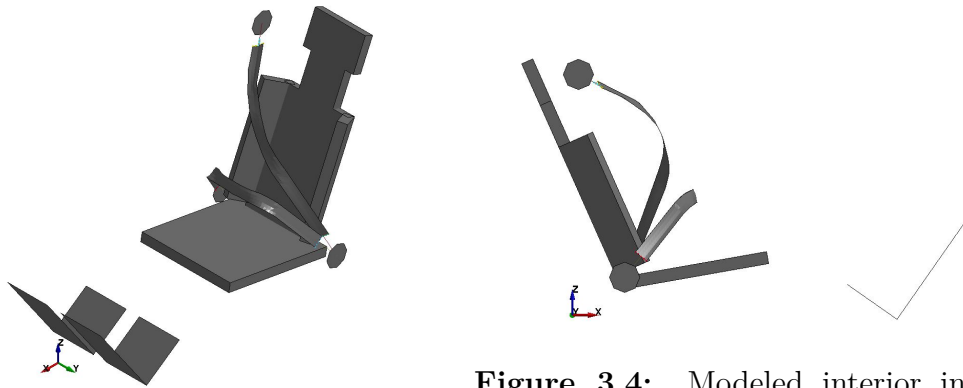


Figure 3.3: Modeled interior in isometric view

Figure 3.4: Modeled interior in xz plane

seat back were created with angle of 120 degrees relative to the seat back according to Huber et al. (2015). Headrest geometry was plotted by extrapolating from the seatback to an estimated distance. The exact shape of the headrest was indifferent, since the contact between the head and the head rest was insignificant in all three maneuvers and this gave few influence to the occupant kinematics.

Seat Mesh Creation: Mesh was created in LS-PrePost and its isometric view was shown in Figure 3.5. The foam was meshed with 8-node solid elements, 40mm. On top of foam there was a layer of shell elements for the cover. On the bottom of the foam there was a layer of shell elements for the bottom plates. The shell elements shared nodes with the foam elements. There was not extra layer of elements for the layer of light-absorbing material.

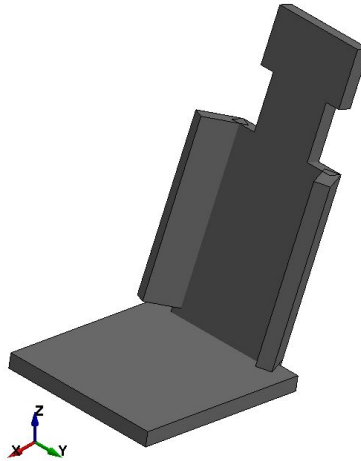


Figure 3.5: Modeled seat in isometric view

Seat Material Properties: Material properties of seatpan bottom and seatback bottom were the same as steel (elastic modulus = 210 GPa, density = 7.0×10^{-6} kg/mm³, Poisson ratio = 0.3). The reason was that no information about the properties of the bottom wooden plate was given and there should not be much deformation from the bottom. Even though those two bottoms were made of wooden

plate in the experiment. For properties of the foam material, the writer took advantage of foam properties from seat of a Ford Taurus car and scaled its stress-strain to a extent that noticeable deformation appeared (the maximum deformation in the seatpan was around 50 %). Material used for cushion on top of the foam was null material (*MAT_NULL in LS-Dyna) in order to improve contacts. The cushion stiffness and mass were neglected.

3.3.2 Seat Belt

Seat Belt Geometry: There was not much information about the seat belt from Huber et al. (2015). Only several words stating a standard 3-point seat belt was used. Nor mentioned they type and properties of the seat belt, neither they gave the exact position of seat belt attachment points and information about pull out of the belt during the experiment. Only belt force during brake event was available from the raw data. Dimension of created belt was $47.5 \times 1.25\text{mm}^2$ for the cross section. Length of shoulder belt and lap belt depended on the position of the seat belt attainment points. Two belts were stretched to fit the body shape of SAFER A-HBM in original position. Torso and lap seat belt had 150mm 1D belt elements at two ends and connected to center of seat belt attachments separately. There was not slip ring for connecting the shoulder seat belt and lap seat belt.

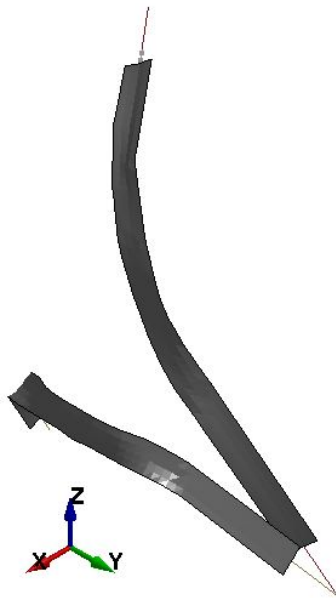


Figure 3.6: Shoulder seat belt and lap seat belt with line elements and spring elements at two ends

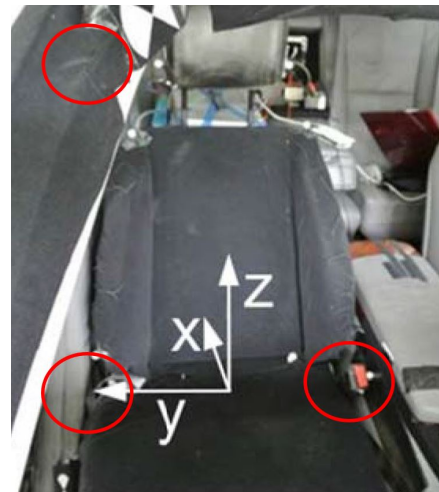


Figure 3.7: Seat in experiment from Huber et al. (2015)

Seat Belt Attachment: Position of three attachment for seat belts was decided based on its estimated position in Figure 3.7. Two lower attachment points were placed 70 mm beside the intersection of the seatpan and seatback. For upper attachment point, a possible attachment position was estimated according to a normal position, since it couldn't be seen from Figure 3.7.

Seat Belt Mesh Creation: Shell elements were used for seat belts. 1 D line elements were used for strings at two belt ends. Two discrete elements were added to the 1 D line elements at the upper corner of lap belt to imitate the belt slack.

Material Properties: Belt material properties were chosen to be representative of a generic seat belt, taken from previous work by Eliasson and Wass (2015). It did not really matter if the belt fabric properties were exactly the same as what was used in the experiment, since deformation of the belt itself would be very small compared to pull out of the belt and belt slack between body and belt. Even film spool effect could be more dominant than the deformation. Two discrete elements at the end of the diagonal belt acted as two springs. One was used as load limit, the other one was used as compensation for belt slack and film spool. Seat belt attachments were modeled with rigid material, because in reality they were metal parts and attached to frame of the car. Center of the seat belt attachments shared nodes with the seat belt line elements.

Seat Belt Slack Tuning: This section discussed how to achieve a similar occupant torso displacement as in experiments, since there was no information about film spool effect and pull out of the seat belt in the publications. The original seat belt appeared to be tight. Therefore, the spring elements at the upper part of the shoulder belt were modified to make the sternum displacement of the SAFER A-HBM magnitude within the experimental corridor. The stiffness was tuned to compensate the belt slack between body and belt and possible film spool effects.

Two offsets to original force - displacement curve were done. By offsetting the force - displacement curve of the spring to the x positive, a softer spring could be achieved, see Figure 3.8. For example for the 40 mm offset, it was done by changing the coordinate of second point from (15, 0.01) to (55, 0.01). There would be linear increase of the stiffness between the (0, 0) and second point.

Three simulations with different force - displacement curves were run to compare the forward displacement of the torso center (Δr_x^{torso}) with the experiment data in brake event.

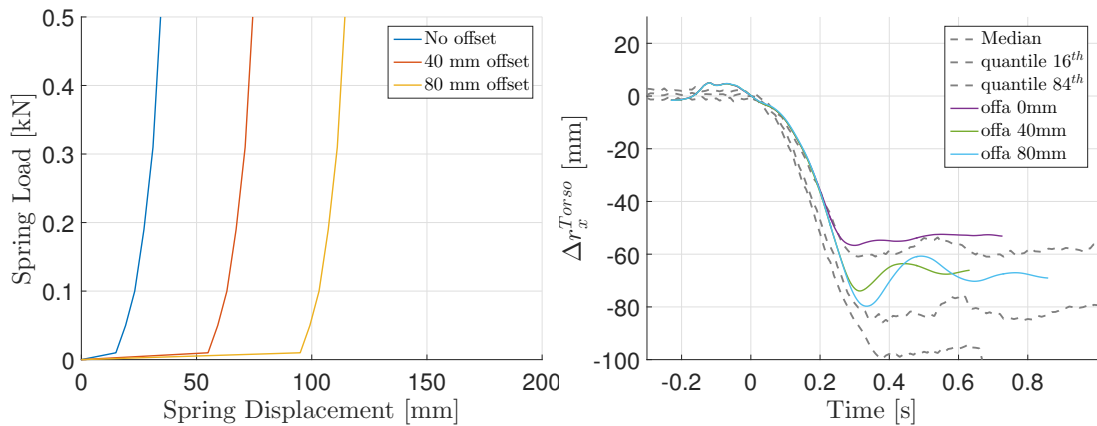


Figure 3.8: Three spring stiffness at 0 mm, 40 mm and 80 mm offsets **Figure 3.9:** Torso displacement Δr_x^{torso} for three spring stiffness

Three setups were tried, one was zero offset for force - displacement curve in film effect spring, one was 40 mm offset, and the other one was 80 mm offset. From the

Figure 3.9, it could be seen that the zero offset setup was located out of the 16th quantile curve. The setups of 40mm and 80mm offsets were both located inside the one standard deviation corridor and was close to each other in the balance position, but the 80 mm offset appeared to be more oscillating. Thus, 40mm offset was selected.

3.3.3 Foot Support

Foot support was positioned under the feet of SAFER A-HBM at its original position. The position and angle of the foot pedal and pedal rest were chosen to be able to make the feet align with the foot support. There was limited information about the foot pedal and pedal rest, e.g. geometry and position of them. Reader should keep in mind that the angle of the foot support could influence the forces acting on the feet and then influence the torso movement.

Geometry: The foot pedal was 200 mm wide and 400 mm long. The pedal rest was square shape with side length 200 mm. Thickness was 1 mm for both.

Mesh: The foot pedal and the pedal rest were meshed with 20 mm times 20 mm shell elements.

Material Properties: Exact material property of the foot pedal was unknown, but it was something hard that can support volunteer's feet. Thus, steel material with density $7.6 \times 10^{-6} \text{kg/mm}^3$ and Young's modules 210 GPa were used.

3.3.4 Positioning

Positioning time was needed to make the SAFER A-HBM fall down to seat and reach suitable stress distribution over the body in sitting position before the loading was applied. The SAFER A-HBM was positioned around 5mm (shortest distance) above the seatpan and around 6 mm (shortest distance) in front of the seat back in the sagittal plane. The positioning time should be long enough to reach a balanced position and short enough for computational convenience. Figure 3.10 shows Δr_x^{Torso} of SAFER A-HBM during the falling down on the seat with and without global damping. There was no loading applied. To reduce computational time, one stimulation with 0.15 global damping factor was run to reduce oscillation of torso center, which could be seen from Figure 3.10. However, numerical problem occurred when global damping factor was not zero and reason hadn't been found out due to limited time.

The positioning time was decided to be 241 ms, because the hands had fallen down to the top of knees after around 200 ms and the torso center displacement in x direction was close to the balanced position. Difference of several milliseconds would not make much divergence.

3.3.5 Load Case

For curves of different load scenarios, please check Figure B.1 for load case brake, Figure B.2 for load case lane change right, and Figure B.3 for load case combined change right.

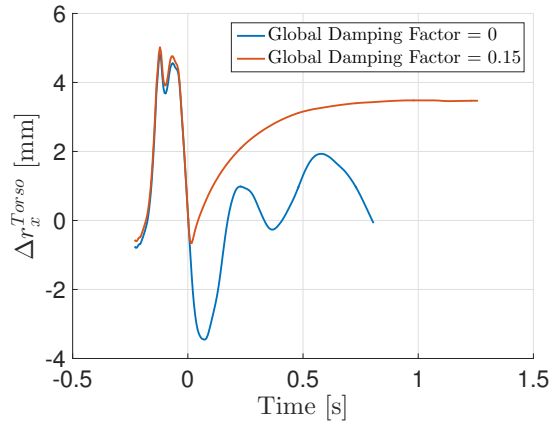


Figure 3.10: Torso center displacement in x axis at global damping factors 0 and 0.15

For the brake event, load scenario data was from raw data provided by Huber et al. (2015). For lane change right event and combined right event, the median acceleration curve from publication (Huber et al., 2015) was taken. 25 subjects' kinematics in different load cases were collected and corresponding corridors were created.

The lane change left maneuver and combined left maneuver were not chosen and analyzed in this study, because people would avoid their head to touch the recording cameras on the right side and occupant kinematics was affected.

There was a positive value at 1.5 s in acceleration curve of brake event (figure B.1), meaning the car was speeding up, which was unrealistic during pre-crash. So the curve after 1.5 s in brake event was discarded for running simulations. The positive part of acceleration curves in lane right event and combined right event were also discarded.

For the braking maneuver, motion of interior was only possible in x axis. Load was applied on seat bottom steel plate, foot support, and belt attachments. When simulation started, interior accelerated in the negative driving direction according to load scenario.

For the lane change maneuver, motion of interior was only in y axis. When positioning time ended, acceleration of the testing vehicle was applied on the interior. The possibly existing x acceleration in reality was neglected for the lane change event.

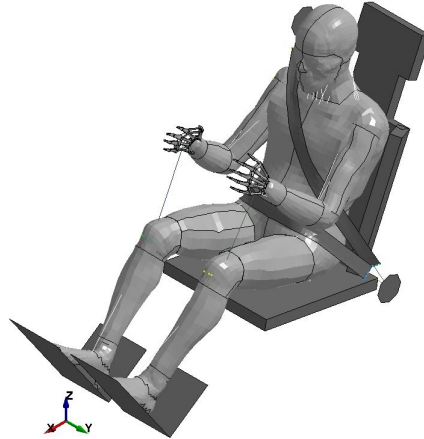
For the combined change maneuver, the motion of the interior was locked only in the z axis. So acceleration curves of testing vehicle in both x and y axes were applied on the interior at the same time.

The summary of constraint directions for all three maneuvers were listed in Table 3.1. The SAFER A-HBM in the interior was shown in Figure 3.11, indicating the coordinate system.

Frame of reference was moving together with the car interior. In simulations, there was no initial velocities for the car interior and SAFER A-HBM. Only load was applied. While in volunteer testing, vehicle had an initial velocity of 50 kph and then different maneuvers started.

Table 3.1: Prescribed direction for three maneuvers

	Prescribed Direction	Locked Direction
Braking Maneuver	x Axis	y and z Axes
Lane Change Maneuver	y Axis	x and z Axes
Combined Change Maneuver	x and y Axes	z Axis

**Figure 3.11:** The SAFER A-HBM in the interior, indicating the coordinate system

3.3.5.1 Constraints of the Hands

Hands were attached to the top of the legs throughout the simulation after initialization. This was because during the experiment volunteers were instructed to not grab the handle on the door. They either put their hands on or beside their legs. This was done by using a combination of re-tractor and pretensioner, which were fixed in the leg on one side and in the hands on the other side. After simulation started, the re-tractor and pretensioner would contract and pull the hands back to the legs.

3.3.5.2 Applying the Acceleration Load

The seatpan bottom and foot support were given a prescribed acceleration, defined in Appendix B. A node list was created for seatpan bottom plate and foot support using keyword `*SET_NODE_LIST` in LS DYNA. After that, keyword `*BOUNDARY_PRESCRIBED_MOTION_SET` for the node set was used to restrict their movement in the direction of defined vector. Direction of the vector was the same as the direction of vehicle acceleration loading during each maneuver.

Same constraint as the seat and foot support was applied on seat belt attachment disks, achieving same movement as the other parts. Because seat belt attachment disks were applied rigid material, which was different from the steel material of seat bottom plate and foot support. Constraint keyword file for attachments could directly use `*BOUNDARY_PRESCRIBED_MOTION_RIGID` without setting node list.

3.4 Output Parameters

For brake event, volunteer kinematics were from raw data provided by Huber et al. (2015). For lane change right event and combined right event, the volunteer kinematics were depicted based on the figures in Huber et al. (2015).

Kinematic parameters were calculated for the SAFER A-HBM using nodal values according to Table 3.2. LS-PrePost macro command code for outputting the X, Y, Z coordinates of each node can be found in Appendix A.2.

Table 3.2: Node number for calculating kinematic parameters

Node Number	8152925	8252925	8885602	8925066	8990011	8990051	43700101
Position	Right Femoral Head	Left Femoral Head	Top of Head	Sternum, Same Height as T5	Spine T1	Spine T5	Head COG

Seat belt force was measured based on average force of three 1D line elements at upper shoulder belt (SB-3520, SB-3521, SB-3522), left side of the lap belt (SB-3502, SB-3503, SB-3504), and right side of the lap belt (SB-3497, SB-3498, SB-3499).

Definition of head and torso displacement, vector, and rotating angle was the same as the description in Huber et al. (2015). For parameter Φ^{Torso} , vector was from H point to the torso center (interpolation between node 8925066 and node 8990051) and for the parameter Φ^{Head} , vector was from torso center and pointed at head COG. While vector for the ϕ^{Torso} was from torso center to a node that was above torso center in original position. Vector for ϕ^{Head} was from head COG to a node (node 8885602) above head COG. Reader should keep in mind that Φ was defined opposite to the ϕ .

Coordinate system in simulations was: origin of Cartesian coordinate system was at the H point of seat, x positive was to the front of the car, y positive was pointing at the left of the passenger, z positive was to the negative gravity.

Definition of y positive in SAFER A-HBM was opposite to the experiment definition, since the the SAFER A-HBM needed to be positioned at its coordinate system to make the controllers working. Kinematic parameters in y direction obtained from SAFER A-HBM had been multiplied a minus sign in order to have the same definition as the experiment corridor.

3.5 Biofidelity Score Calculation - CORA

CORA (CORrelation and Analysis) provided an objective evaluation of time-history signals and was used here to evaluate the relevance between the SAFER A-HBM simulation results and the volunteer tests. A corridor rating and a cross-correlation rating were used together in CORA (ISO/TS 18571:2014(E), 2014). The weight for user defined corridor and default CORA corridor was both 0.5 in this study, the weight for corridor rating and cross-correlation rating were both 0.5. Only time

range 0 - 630 ms was used to do the CORA since the shortest simulation time was 630 ms.

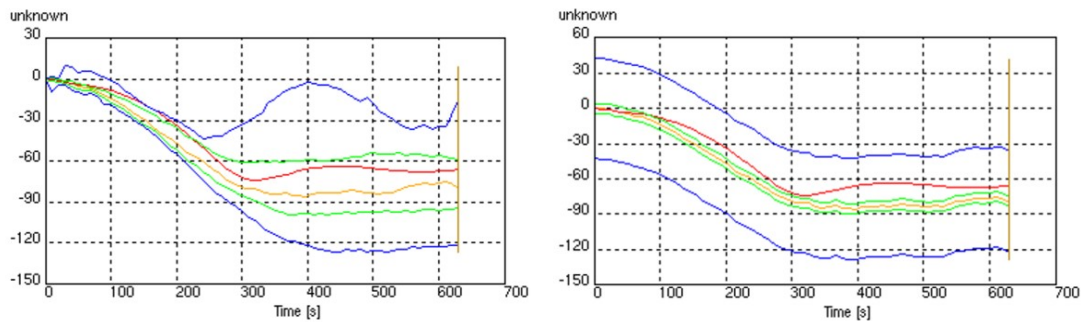


Figure 3.12: User defined corridor. **Figure 3.13:** Default CORA corridor. Read line was comparison curve. Green Read line was comparison curve. Green lines formed inner corridor. Blue lines lines formed inner corridor. Blue lines formed the outer corridor. formed the outer corridor.

3.6 Simulation Summary

Different settings were investigated in order to find out the influence to the performance of the SAFER A-HBM during different conditions, such as passive SAFER A-HBM, a different seat, and an interior model without foot support.

Motivation to implement the passive SAFER A-HBM was to investigate how much improvement could be reached after the omnidirectional active muscles were implemented.

In order to find out how the kinematic response would change when another seat was used, a Ford Taurus seat from National Crash Analysis Center (George Washington University, USA) was simulated for comparison. The Taurus seat used in this study didn't have head restraint.

To investigate influence of activation level of leg muscles towards the occupant kinematics, interior without foot support was simulated. Since rotation around knee was locked in SAFER A-HBM, changing the activation level in leg muscles would not affect leg movement. Thus, no foot support setup was used to approximate zero activation of thigh muscles, since no contact force would be generated from the feet to stop SAFER A-HBM to lean forwards. Even though this couldn't be exactly same as zero activation level of leg muscles with rotatable knee joints.

In Table 3.3, three simulations (Sim 1 - Sim 3) showed the settings for the simulations of SAFER A-HBM in three different maneuvers, according to the Section 3.3.5 above.

Sim 4 - Sim 6 showed the settings for the simulations in different maneuvers with muscle element but without muscle activation.

Sim 7 - Sim 9 showed the settings for the simulations of SAFER A-HBM on Taurus seat.

Sim 11, Sim 1 and Sim 12 showed the settings in tuning the belt slack. For curves of spring stiffness at different offset, please see Figure 3.8. Sim 13 showed settings

3. Methods

for simulations of SAFER A-HBM without foot support.

Table 3.3: Simulations matrix

Simulation Name	Simulation Model	Interior Model	Load Event	Neck and Trunk Hill Type Muscle Activation	Upper and Lower Extremities Hill Type Muscle Activation	Stiffness Curve
Sim 1	SAFER A-HBM	Testing Seat	Brake Event	Yes	No	40 mm Offset
Sim 2	SAFER A-HBM	Testing Seat	Lane Change Right Event	Yes	No	40 mm Offset
Sim 3	SAFER A-HBM	Testing Seat	Combined Change Right Event	Yes	No	40 mm Offset
Sim 4	SAFER A-HBM	Testing Seat	Brake Event	No	No	40 mm Offset
Sim 5	SAFER A-HBM	Testing Seat	Lane Change Right Event	No	No	40 mm Offset
Sim 6	SAFER A-HBM	Testing Seat	Combined Change RightEvent	No	No	40 mm Offset
Sim 7	SAFER A-HBM	Taurus Seat	Brake Event	Yes	No	40 mm Offset
Sim 8	SAFER A-HBM	Taurus Seat	Lane Change Right Event	Yes	No	40 mm Offset
Sim 9	SAFER A-HBM	Taurus Seat	Combined Change Right Event	Yes	No	40 mm Offset
Sim 10	SAFER A-HBM	Testing Seat without Foot Support	Brake Event	Yes	No	40 mm Offset
Sim 11	SAFER A-HBM	Testing Seat	Brake Event	Yes	No	0 mm Offset
Same as Sim 1	SAFER A-HBM	Testing Seat	BrakeEvent	Yes	No	40 mm Offset
Sim 12	SAFER A-HBM	Testing Seat	Brake Event	Yes	No	80 mm Offset
Sim 13	SAFER A-HBM	Testing Seat	Gravity	Yes	No	40 ?mm Offset

4

Results

4.1 Kinematic Comparisons of SAFER A-HBM

Table 4.1 was a summary of the compared parameters of SAFER A-HBM under three different maneuvers (Sim 1 - Sim 3).

Table 4.1: Summary of qualitative assessment

	A-HBM	Experiment
Braking	$\Delta r_x^{Torso}, \Delta r_x^{Head}, \Phi_y^{Torso}, -\Phi_y^{Torso} - \phi_y^{Torso}, \phi_z^{Torso}, \phi_z^{Head}, \text{belt force}$	
Lane Right	$\Delta r_y^{Torso}, \Delta r_y^{Head}, \Phi_x^{Torso}, -\Phi_x^{Torso} - \phi_x^{Torso}$	
Combined Right	$\Delta r_x^{Torso}, \Delta r_x^{Head}, \Delta r_y^{Torso}, \Delta r_y^{Head}$	

4.1.1 Brake Event

In this section, comparison between SAFER A-HBM and experimental data of following parameters were showed: $\Delta r_x^{Torso}, \Delta r_x^{Head}, \Phi_y^{Torso}, -\Phi_y^{Torso} - \phi_y^{Torso}, \phi_z^{Torso}, \phi_z^{Head}$, and belt force. Simulation ran for 870 ms (Sim 1) and then reported an error termination due to numerical problem, which was negative volume in an element around cervical spine area.

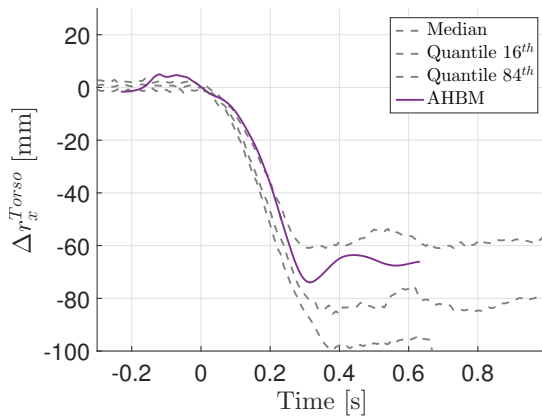


Figure 4.1: Torso displacement Δr_x^{Torso} of SAFER A-HBM during brake event.

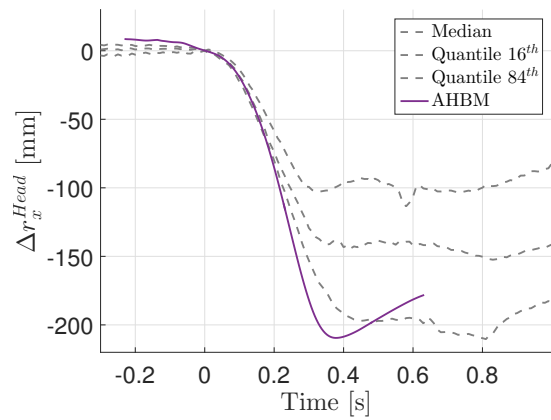


Figure 4.2: Head displacement Δr_x^{Head} of SAFER A-HBM during brake event

4. Results

Figure 4.1 showed that Δr_x^{Torso} located between median curve and quantile 16th curve. Figure 4.2 showed that Δr_x^{Head} located roughly at the position of the quantile 84th curve, which meant it was at the edge of the one σ corridor. During time 0-300 ms, SAFER A-HBM results matched the experiments well when occupants were leaning forward.

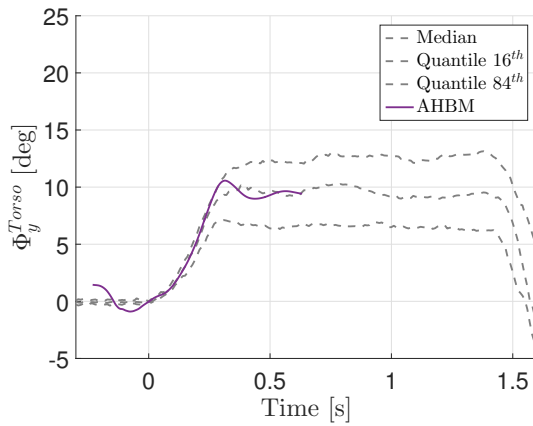


Figure 4.3: Torso angle change Φ_y^{Torso} of SAFER A-HBM in brake event.

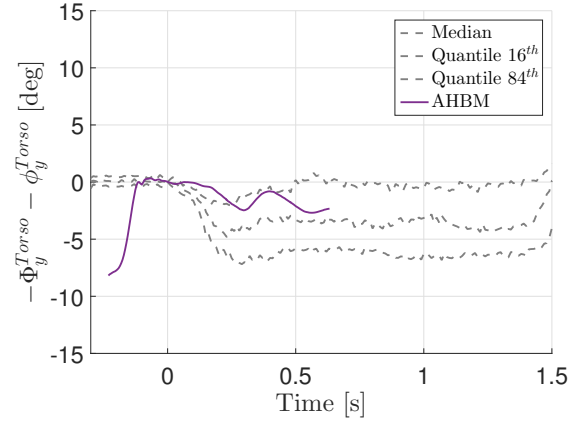


Figure 4.4: Torso bending angle $-\Phi_y^{Torso} - \phi_y^{Torso}$ of SAFER A-HBM in brake event.

Figure 4.3 and Figure 4.4 showed that both Φ_y^{Torso} and $-\Phi_y^{Torso} - \phi_y^{Torso}$ were located inside the one standard deviation corridor.

The reason for difference between the A-HBM and experimental regarding Φ_y^{Torso} and $-\Phi_y^{Torso} - \phi_y^{Torso}$ could come from some slide between hip and seat. So H point and torso center would both have some forward displacement and thus, rotation angle was not that big.

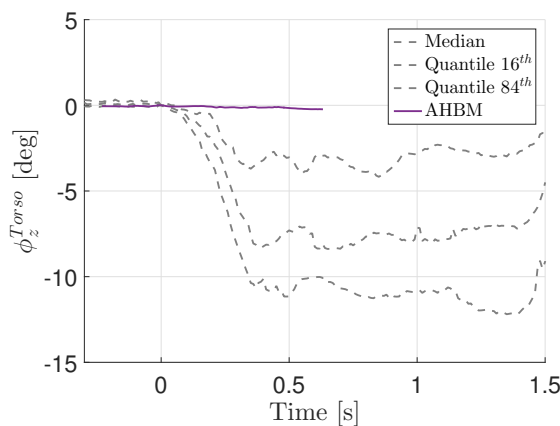


Figure 4.5: Torso rotation angle ϕ_z^{Torso} of SAFER A-HBM in brake event.

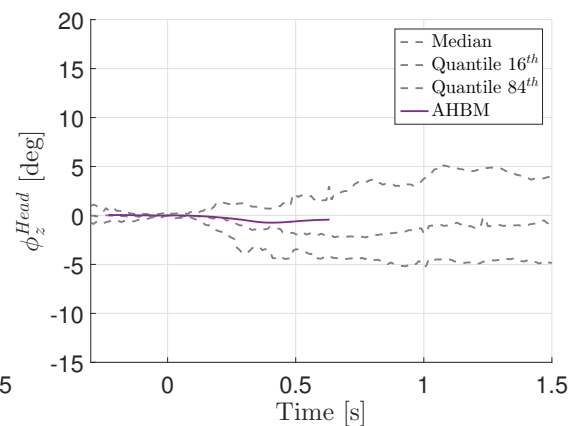


Figure 4.6: Head rotation angle ϕ_z^{Head} of SAFER A-HBM in brake event.

Torso rotation angle around z axis was very small, showed in Figure 4.5 While the volunteers' rotation showed around 7 deg due to the asymmetric of the three point

seat belt. There was also not much rotation in z axis for the head (figure 4.6). Volunteers' corridor was surrounding the 0 deg, so it located inside the one sigma corridor.

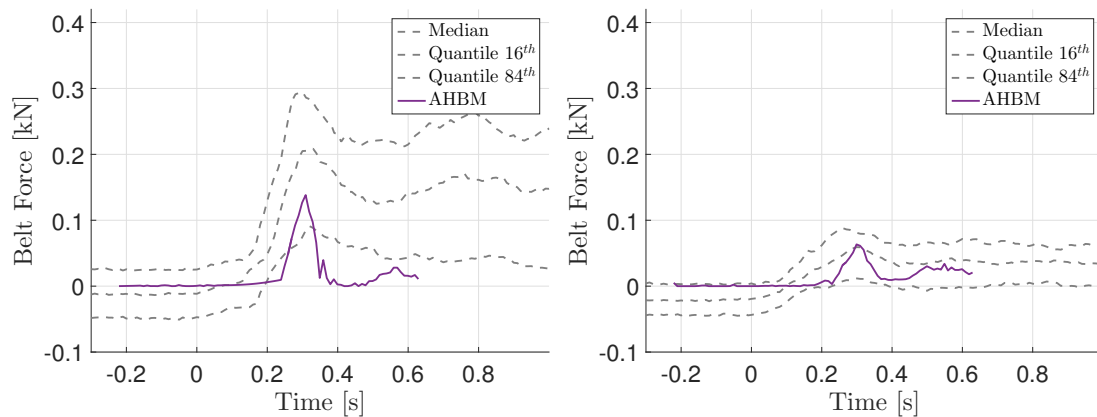


Figure 4.7: Shoulder belt force of SAFER A-HBM in brake event.

Figure 4.8: Lap belt force of SAFER A-HBM in brake event.

Figure 4.7 and 4.8 showed shoulder belt force and lap belt force.

For shoulder belt force, it reached peak force 0.138 kN at $t = 0.309$ s, then it dropped to 0.002 kN at $t = 0.379$ s. After that, it went up to 0.028 kN at 0.559 s and then showed a decreasing trend. It could be seen that the shoulder belt force curve located quite far from the median and after 0.329 s, the curve were located outside the one standard deviation corridor. For lap belt force, force started to slightly go up to 0.0016 kN at $t = 0.149$ s. After that, force peaked at 0.063 kN at $t = 0.299$ s. Then went down to 0.009 kN at $t = 0.399$ s and rose again to 0.03 kN at $t = 0.499$ s. Later it fluctuated there around 0.03 kN. Whole lap belt force located inside the one standard deviation corridor.

Shoulder seat belt and lap seat belt were independent to each other in simulation settings. In reality, shoulder belt and pelvic were one belt that went through slip ring and a balance could be made between the torso part and pelvic part. One simulation using slip ring was done to find out if the two independent seat belts deviated much from reality. The results showed that relative movement between the seat belt and slip ring was less than a length of one element. Shoulder seat belt force and lap seat belt force had similar curve shape as without slip ring, but the shoulder belt force peaked at 0.1 kN and the lap belt force peaked at around 0.09 kN. Few difference in body motion was observed between with slip ring and without slip ring.

The time that the force peaked were almost the same as the experiment, which showed in another way that the torso reached the max displacement at a similar time as Δr_x^{Torso} showed. For the reason that the shoulder belt force deviated from the experiment corridor, it may come from the low friction between seat and volunteers.

4.1.2 Lane Change Right Event

In this section, comparison between SAFER A-HBM and experimental data were showed in the following parameters: Δr_y^{Torso} , Δr_y^{Head} , Φ_x^{Torso} , $-\Phi_x^{Torso} - \phi_x^{Torso}$. Sim 2 terminated normally at 2 300 ms.

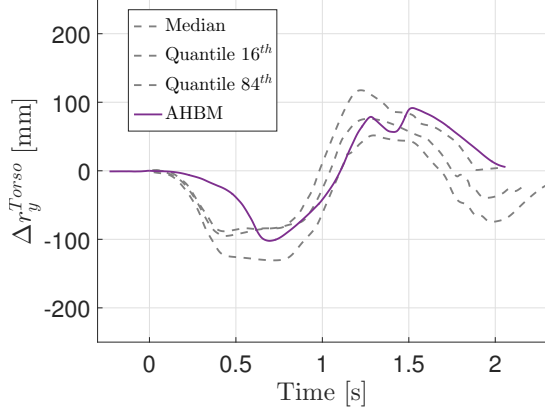


Figure 4.9: Torso displacement Δr_y^{Torso} of SAFER A-HBM in lane right event.

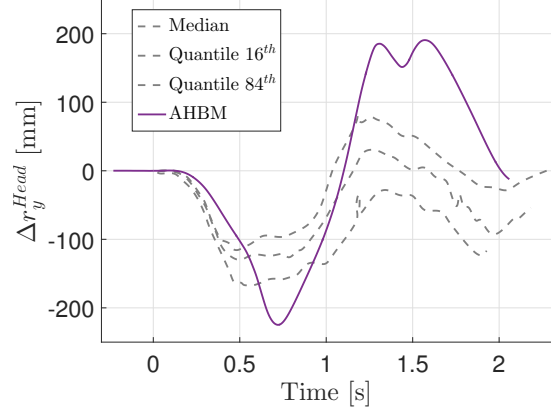


Figure 4.10: Head displacement Δr_y^{Head} of SAFER A-HBM in lane right event.

Figure 4.9 and Figure 4.10 showed torso and head displacement in y direction. The torso displacement in y direction followed the one σ corridor, while the head displacement in y direction exceeded the corridor at the range around peak.

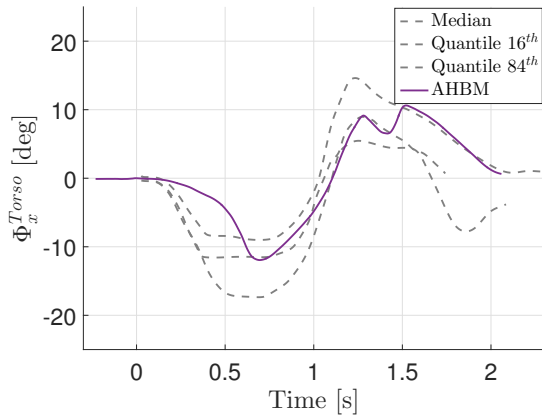


Figure 4.11: Torso angle change Φ_x^{Torso} of SAFER A-HBM in lane right event.

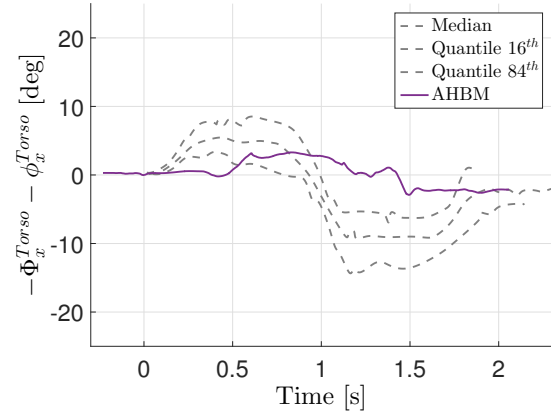


Figure 4.12: Torso bending angle $-\Phi_x^{Torso} - \phi_x^{Torso}$ of SAFER A-HBM in lane right event.

Figure 4.11 and Figure 4.12 showed two different bending to the side direction, Φ_x^{Torso} and $-\Phi_x^{Torso} - \phi_x^{Torso}$. Parameter Φ_x^{Torso} followed the corridor well after the first 600 ms. Parameter $-\Phi_x^{Torso} - \phi_x^{Torso}$ appeared to be different from the corridor, with few correlation in the shape.

Three parameters, Δr_y^{Torso} , Δr_y^{Head} , and Φ_x^{Torso} , had lags during 0 - 600 ms. That might be because friction of the seat was low. The friction factor was 0.3 in this study.

From simulation animation, obvious slide in y direction between SAFER A-HBM and seat could be observed when loading changed direction. The slide may come from a small enough friction coefficient or the unsuitable deformation property of the seat foam and resulted in deviation from the corridor for bending of the torso $-\Phi_x^{Torso} - \phi_x^{Torso}$.

The concave appearing at time 1 200 ms was because the upper belt slid off from the shoulder and slid onto the shoulder. During experiment, volunteers would shrug their shoulders to stop the slide of the seat belt when they felt there was a possibility of sliding. However, this was not simulated by the SAFER A-HBM.

4.1.3 Combined Change Right Event

In this section, figures would show difference between the SAFER A-HBM simulation and experiment data regarding the combined right maneuvers. Sim 3 ran for 1252 ms and met error termination. Error was triggered by complex sound speed at element 8740038 and element 8740052, which were located in the cervical spine area.

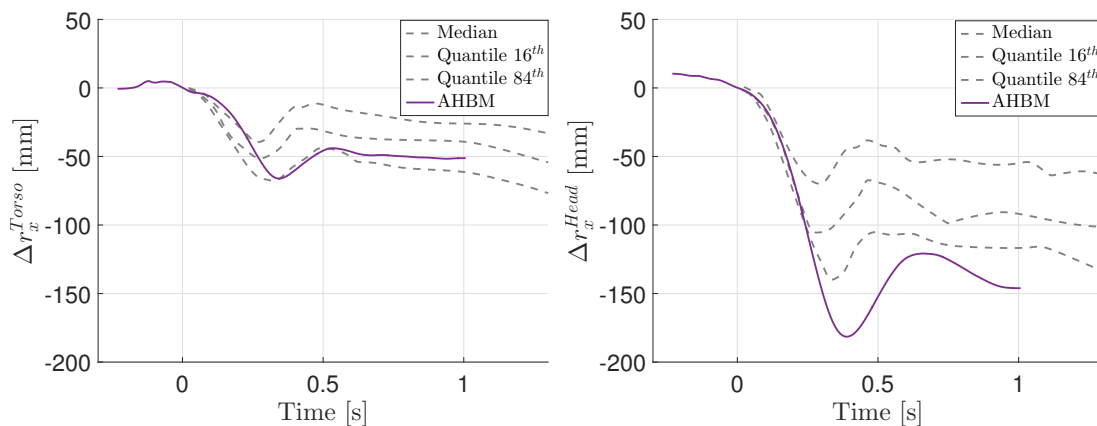


Figure 4.13: Torso displacement Δr_x^{Torso} of SAFER A-HBM in combined right event. **Figure 4.14:** Head displacement Δr_x^{Head} of SAFER A-HBM in combined right event.

Figure 4.13 and Figure 4.14 showed displacement of head COG and torso center in x direction. After $t = 0$ s, Δr_x^{Torso} continued decreasing and reached -66.12 mm at $t = 0.342$ s. Then it went up again and peaked at -43.98 mm at $t = 0.537$ s. After that, it slowly went down to -51.23 mm at $t = 1.007$ s. Δr_x^{Head} showed a similar shape of curve with larger magnitude. From $t = 0$ s, the Δr_x^{Head} dropped from 0 mm to -181.5 mm at $t = 0.187$ s. Afterwards, it increased again to -120.8 mm at $t = 0.657$ s. Then decreased to -146.1 mm at $t = 1.007$ s. Compared with Figure 4.11, peak point of Δr_x^{Torso} located inside the quantile 84th curve, which was -66.12 mm compared to around -75 mm. For Δr_x^{Head} , peak point (-181.5mm) went below -140 mm, which meant it was outside the curve of the quantile 84th.

Parameter Δr_x^{Torso} showed a little lag in the first 300 ms, then simulation result was very close the edge of the quantile 84th curve. While parameter Δr_x^{Head} showed no lag in the beginning, its peak exceeded the corridor for about 50 mm, meaning neck muscle needed to be improved when a lateral loading was combined with frontal one.

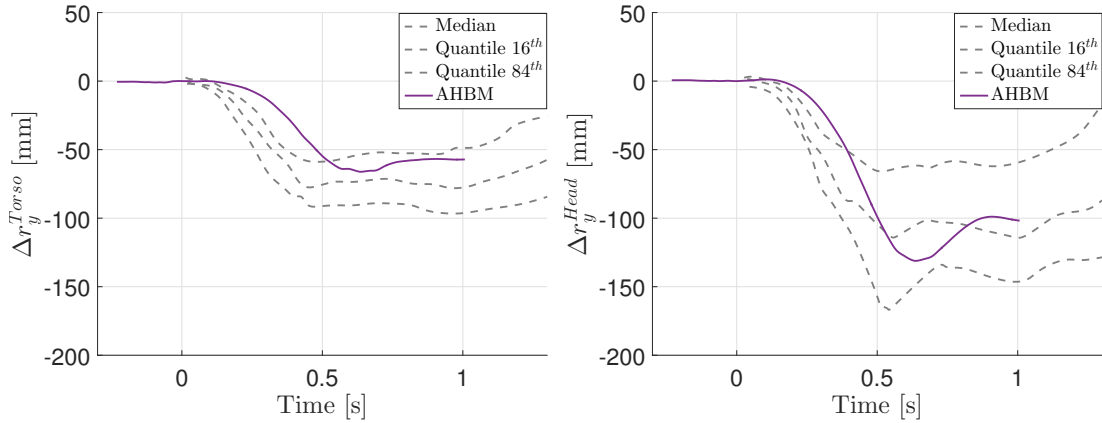


Figure 4.15: Torso displacement Δr_y^{Torso} of SAFER A-HBM in combined right event. **Figure 4.16:** Head displacement Δr_y^{Head} of SAFER A-HBM in combined right event.

Figure 4.15 and 4.16 showed displacement of the head COG and the torso center in y direction. After $t = 0$ s, the Δr_y^{Torso} continued decreasing and reached -66.18 mm at $t = 0.637$ s, then it went up again and reached a platform until $t = 1.002$ s at -43.98 mm. Δr_x^{Head} showed a similar shape of curve with larger magnitude. From $t = 0$ s, Δr_x^{Head} dropped from 0 mm to -131.2 mm at $t = 0.637$ s. After that, it increased again to -98.92 mm at $t = 0.907$ s. Then decreased to -101.8 mm at $t = 1.007$ s. Peak point of Δr_y^{Torso} located inside the quantile 84th curve, which was -66.18 mm compared to around -90 mm. For Δr_y^{Head} , peak point (-131.2 mm) went below -160 mm, which located inside the curve of the quantile 84th.

Lags of simulations compared to experiment corridor appeared for the first 600 ms, which was similar to lags showed in lane change right maneuvers. Only movement in y direction showed the lag instead of in x direction. So the lag may also come from insufficient side support in the numerical simulation, together with the previously discussed possibilities of small friction coefficient and inaccurate foam property.

Displacement in y direction reached its maximum at time later than the x direction, which was the case for both the head and torso during simulation and experiment.

4.2 Modification of Muscle Activation and Interior Model

Table 4.2 was a summary of the compared kinematic parameters for Sim 4 - Sim 13. In this section, different setups were analyzed, such as a passive SAFER A-HBM, SAFER A-HBM on a Taurus seat, and an interior without foot support. Motivation

Table 4.2: Summary of the parameters

	A-HBM	Passive A-HBM	Taurus Seat	No Pedal
Braking	$\Delta r_x^{Torso}, \Delta r_x^{Head}, \Phi_y^{Torso}, -\Phi_y^{Torso} - \phi_y^{Torso}, \phi_z^{Torso}, \phi_z^{Head}$			
Lane Right	$\Delta r_y^{Torso}, \Delta r_y^{Head}, \Phi_x^{Torso}, -\Phi_x^{Torso} - \phi_x^{Torso}$			
Combined Right	$\Delta r_x^{Torso}, \Delta r_x^{Head}, \Delta r_y^{Torso}, \Delta r_y^{Head}$			

for implementing those simulations was stated in the Section 3.6.

4.2.1 Brake Event

Simulation of passive SAFER A-HBM (Sim 4) terminated normally at 1500 ms. Simulation of SAFER A-HBM on Taurus seat (Sim 7) terminated normally at 1100 ms. Simulation of no foot support (Sim 10) ran normally for 1100 ms. The time stating here included the positioning time.

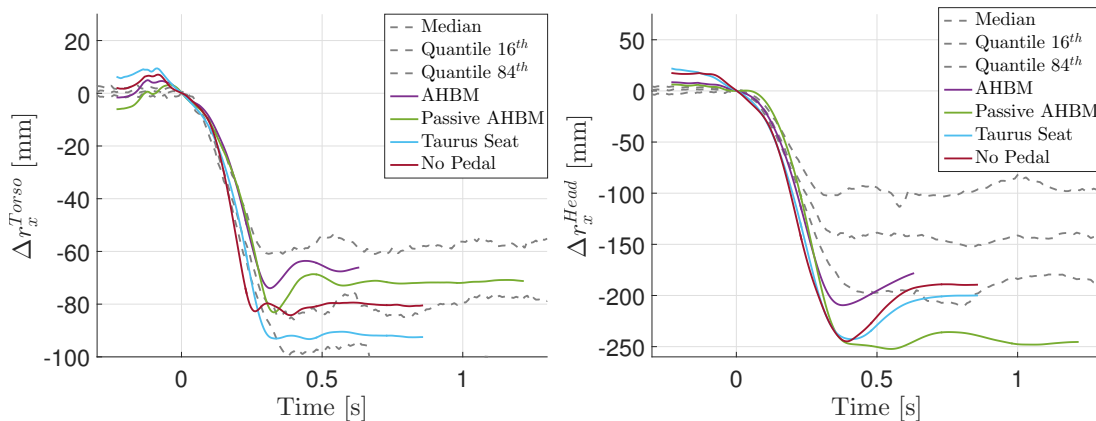


Figure 4.17: Comparison of torso displacement Δr_x^{Torso} during brake event in setups SAFER A-HBM, passive SAFER A-HBM, Taurus seat and without foot support. **Figure 4.18:** Comparison of head displacement Δr_x^{Head} during brake event in setups SAFER A-HBM, passive SAFER A-HBM, Taurus seat and without foot support.

Figure 4.17 showed that simulation of no foot support was the closest curve to the corridor median for torso center displacement. This was due to the existence of slide between hip and seat when there was no foot support. So torso center could move further than the SAFER A-HBM in Sim 1. Taurus seat showed larger displacement due to the softness of the seat pan.

In Figure 4.18, all three human body models with active muscle showed similarity in backward movement of head after Δr_x^{Head} reached peak movement, while passive SAFER A-HBM just stayed in the maximum extent.

Figure 4.19 showed angular change of vector H point to torso center. Reference position was state at the end of positioning time. Order of those four curves was the upside down of them in Δr_x^{Torso} . SAFER A-HBM and passive SAFER A-HBM showed good consistency with corridor median.

4. Results

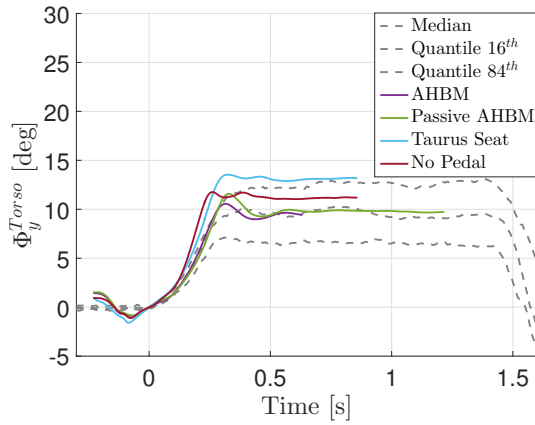


Figure 4.19: Comparison of torso angle change Φ_y^{Torso} during brake event in setups SAFER A-HBM, passive SAFER A-HBM, A-HBM, Taurus seat and without foot support.

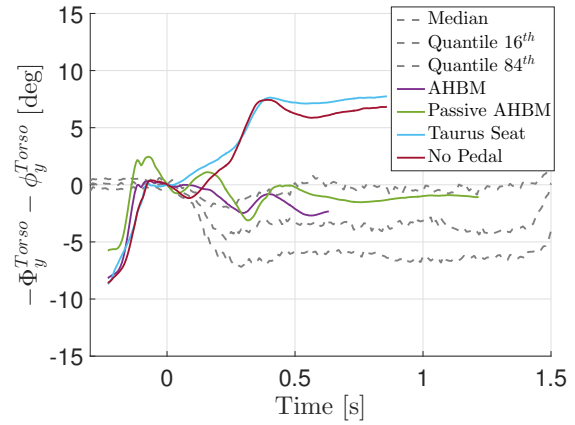


Figure 4.20: Comparison of torso bending extent $-\Phi_y^{Torso} - \phi_y^{Torso}$ during brake event in setups SAFER A-HBM, passive SAFER A-HBM, A-HBM, Taurus seat and without foot support.

Figure 4.20 showed bending extent of the torso segment. SAFER A-HBM and passive SAFER A-HBM were roughly located in the one σ corridor, while Taurus seat setup and no foot support setup showed quite big deviation. This meant that either volunteers were trying to do the extension of their vertebra column or force of seat belt was pushing back the upper torso. For Taurus seat setup and no foot support setup, upper torso was moving forwards larger than the lower part due to deceleration.

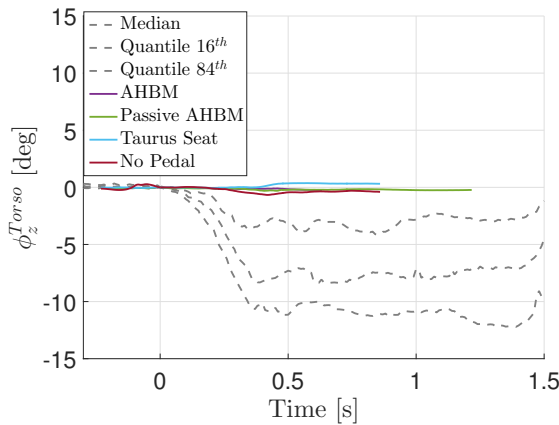


Figure 4.21: Comparison of torso rotation angle ϕ_z^{Torso} during brake event in setups SAFER A-HBM, passive SAFER A-HBM, A-HBM, Taurus seat and without foot support.

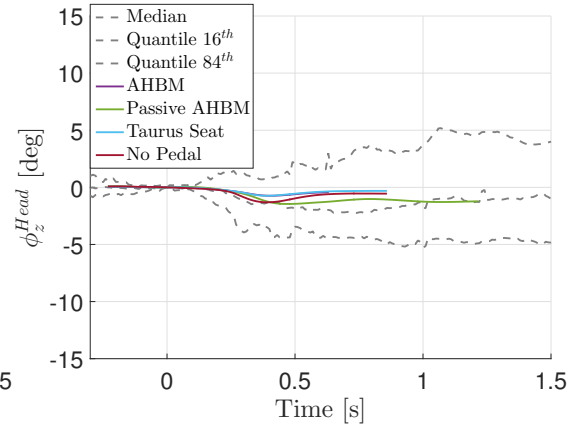


Figure 4.22: Comparison of head rotation angle ϕ_z^{Head} during brake event in setups SAFER A-HBM, passive SAFER A-HBM, A-HBM, Taurus seat and without foot support.

Figure 4.21 showed that little difference could be found between those three different setups. They were all close to 0 degree of rotation in z axis, which meant no turning

in the torso.

In Figure 4.22, SAFER A-HBM was very close to Taurus seat in parameter ϕ_z^{Head} . However, passive SAFER A-HBM and no foot support setups showed slightly difference. They were all located inside the corridor.

4.2.2 Lane Right Event

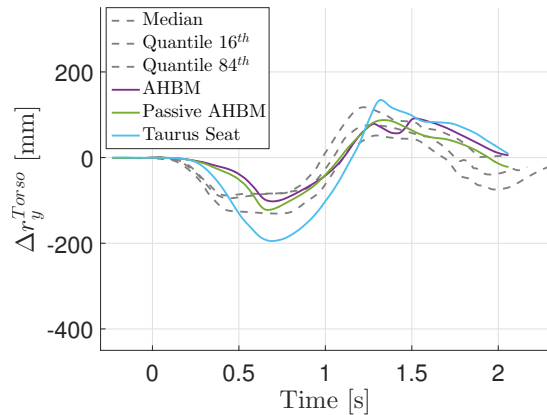


Figure 4.23: Comparison of torso displacement Δr_y^{Torso} during lane right event in setups SAFER A-HBM, passive SAFER A-HBM and Taurus seat.

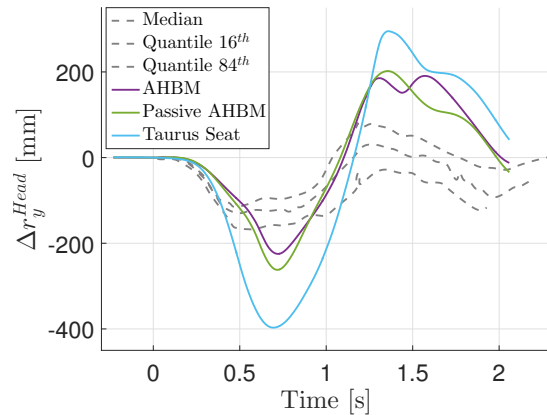


Figure 4.24: Comparison of head displacement Δr_y^{Head} during lane right event in setups SAFER A-HBM, passive SAFER A-HBM and Taurus seat.

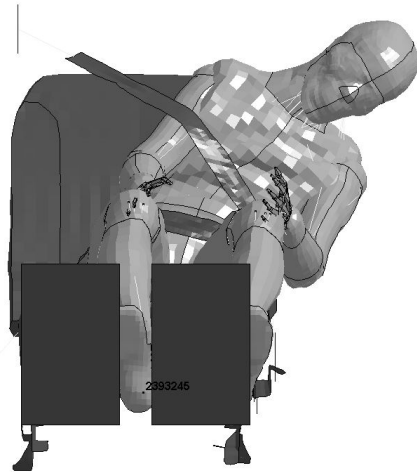


Figure 4.25: Body motion on Taurus seat when the maximum y displacement occurred.

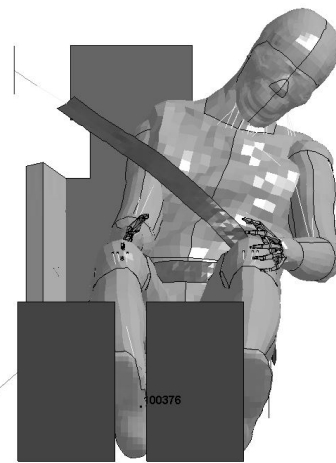


Figure 4.26: Body motion on testing seat when the maximum y displacement occurred.

Figure 4.23 showed torso center displacement in y direction for Sim 2, Sim 5 and Sim 8. Displacements of SAFER A-HBM and passive SAFER A-HBM were inside the corridor after around 600 ms. Displacement of Taurus seat was mostly located outside the corridor. In Figure 4.24, head center displacement curves of SAFER

A-HBM and passive SAFER A-HBM showed better anastomosis with the corridor compared to the Taurus seat. However, their peak value all exceeded double value of the corridor peak. Both figures showed a shift during time 0 - 600 ms for the three curves.

Large displacement in simulation of Taurus seat came from slide of the shoulder belt on the shoulder and there was no side support in the seatback for shoring the body compared to testing seat. So the body motion continued moving to the side on Taurus seat while was stopped by the side support on the testing seat. Figure 4.25 and 4.26 showed the body motion in simulation when SAFER A-HBM on both seats reached the maximum head displacement.

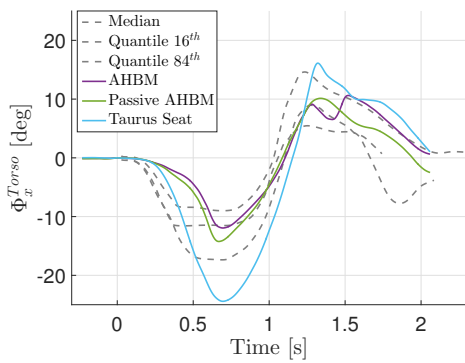


Figure 4.27: Comparison of torso angle change Φ_x^{Torso} during lane right event in setups SAFER A-HBM, passive SAFER A-HBM and Taurus seat.

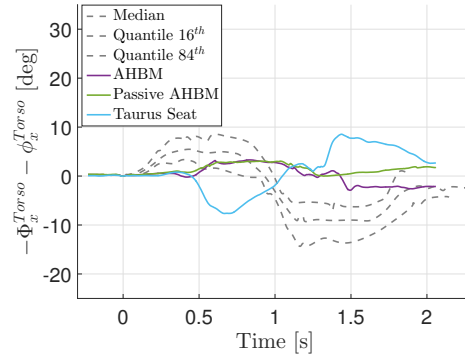


Figure 4.28: Comparison of torso bending angle $-\Phi_x^{Torso} - \phi_x^{Torso}$ during lane right event in setups SAFER A-HBM, passive SAFER A-HBM and Taurus seat.

Figure 4.27 showed rotation of torso center around the hip point. SAFER A-HBM and passive SAFER A-HBM were located inside the one σ corridor after around 600 ms and Taurus seat setup was far below the corridor lower boundary. In Figure 4.28, bending of torso segments to the side in SAFER A-HBM and passive SAFER A-HBM were very close to each other, while Taurus seat setup showed big difference. All the three curves were not so coincident with the experiment corridor. The human body models appeared to be more rigid than the volunteers. Taurus seat curve lied in the area above 0 deg. This probably was because that bending of the upper torso segment was even more towards the side than the lower torso segment without any prevention compared to the testing side.

4.2.3 Combined Right Event

Figure 4.29 and 4.30 showed displacement of torso center and head center in x direction for Sim 3, Sim 6 and Sim 9. All three curves were following the trends of the volunteers' corridor but were outside the lower boundary. SAFER A-HBM showed the best coincides. The torso displacement of passive SAFER A-HBM setup located between Taurus seat setup and SAFER A-HBM setup, while the head displacement of Taurus seat setup located between SAFER A-HBM and passive SAFER A-HBM.

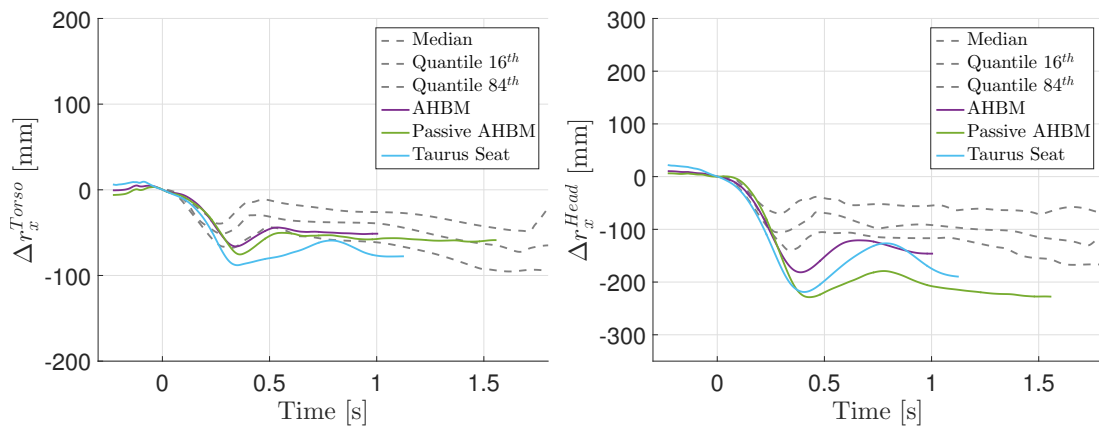


Figure 4.29: Comparison of torso displacement Δr_x^{Torso} during combined right event in setups SAFER A-HBM, passive SAFER A-HBM and Taurus seat. **Figure 4.30:** Comparison of head displacement Δr_x^{Head} during combined right event in setups SAFER A-HBM, passive SAFER A-HBM and Taurus seat.

Figure 4.31 and 4.32 showed displacement of torso center and head center in y direction. With some delays in the first 600 ms, the curves of SAFER A-HBM and passive SAFER A-HBM lied inside the corridor and were more or less close to each other for the both figures. Performance of Taurus seat setup was far below the lower corridor for both torso and head displacements.

4.3 Biofidelity Score - CORA

The Table 4.3 showed the rating in brake event for Sim 1 (with muscle activation) and Sim 4 (passive SAFER A-HBM):

Table 4.3: CORA rating of brake event

	Sim 1 (With Muscle Activation)	Sim 4 (No Muscle Activation)
Δr_x^{Torso}	0.832	0.883
Δr_x^{Head}	0.721	0.580
Φ_y^{Torso}	0.984	0.959
$-\Phi_y^{Torso} - \phi_y^{Torso}$	0.588	0.426

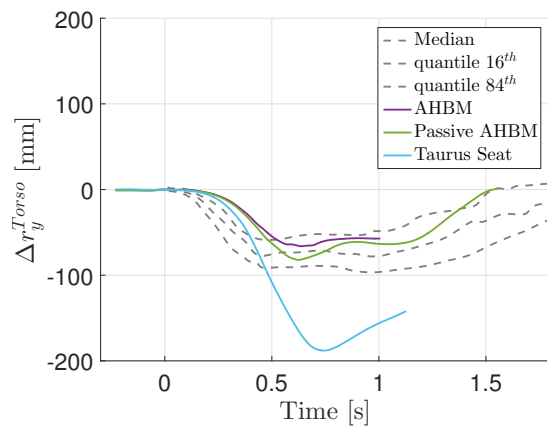


Figure 4.31: Comparison of torso displacement Δr_y^{Torso} during combined right event in setups SAFER A-HBM, passive SAFER A-HBM and Taurus seat.

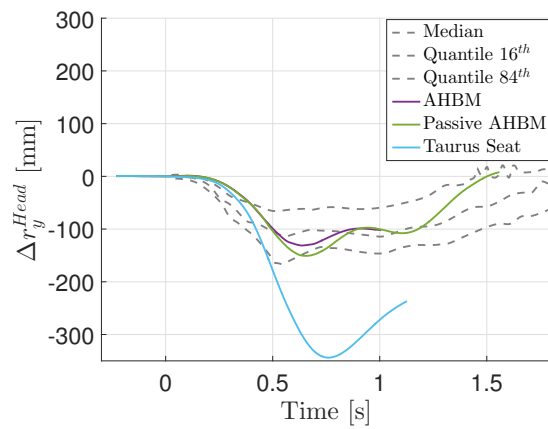


Figure 4.32: Comparison of head displacement Δr_y^{Head} during combined right event in setups SAFER A-HBM, passive SAFER A-HBM and Taurus seat.

5

Discussion

In the visual inspection of SAFER A-HBM, there was obvious slide between the buttock and the seatpan during lane right event and combined right event. It would be good if the H point kinematic data could be compared between the simulations and the volunteer testing. However, the H point movement data was not existing in the raw data.

The side support was also important for affecting the bending of torso segment and displacement of head and torso. However, the details were not available regarding the exact shape of the side support. Thus, the kinematics of the human body model may differ from the volunteers.

Forces generated by arm muscles may influence the upper body kinematics but the SAFER A-HBM has zero activation in the arms. The effects of support of arms on the thighs may need further investigation.

Readers should bear in mind that this study is unable to duplicate the entire experiment setup, because of lacking of information like: seat foam and seat cover material properties, seat belt attachment point position, the pull out distance of the belt, the H point movement, and the position of the foot support. Thus, the study has made assumptions and simplifications on the simulation setup, which may lead to inaccurate results.

It is beyond the scope of this study to eliminate the numerical error termination in some elements due to large deformation and negative element volume in SAFER A-HBM. Some simulations would terminate earlier than the experiment duration. The problem is limited to very few elements and would not affect the correctness of the SAFER A-HBM response.

6

Conclusion

The SAFER A-HBM has better performance than the passive SAFER A-HBM in occupant kinematics, especially in the head kinematics. Compared to experiments, SAFER A-HBM performs well during three maneuvers. Some kinematics parameters lie inside the one standard deviation corridor or on the edge. But the kinematics in the y direction shows some deviation as long as the load has component in y direction. So tuning neck muscles for omnidirection is still needed for future work. The Taurus seat shows much less correlation compared to a testing seat. A different seat contributes to a different occupant kinematics, especially the side supports would influence the motion during lane change maneuver and combined maneuver. The activation level in leg muscles and the belt pull out distance are also important for slide between hip and seat surface.

References

- Administration, N. H. T. S., et al. (2016). 2015 motor vehicle crashes: overview. *Traffic safety facts research note, 2016*, 1–9.
- Arbogast, K. B., Balasubramanian, S., Seacrist, T., Maltese, M. R., Garcia-Espana, J. F., Hopely, T., . . . others (2009). Comparison of kinematic responses of the head and spine for children and adults in low-speed frontal sled tests. *Stapp car crash journal, 53*, 329.
- Arbogast, K. B., Mathews, E. A., Seacrist, T., Maltese, M. R., Hammond, R., Balasubramanian, S., . . . Higuchi, K. (2012). The effect of pretensioning and age on torso rollout in restrained human volunteers in far-side lateral and oblique loading. *Stapp car crash journal, 56*, 443.
- Beeman, S. M., Kemper, A. R., Madigan, M. L., Franck, C. T., & Loftus, S. C. (2012). Occupant kinematics in low-speed frontal sled tests: Human volunteers, hybrid iii atd, and pmhs. *Accident Analysis & Prevention, 47*, 128–139.
- Behr, M., Arnoux, P.-J., Serre, T., Thollon, L., & Brunet, C. (2006). Tonic finite element model of the lower limb. *Journal of biomechanical engineering, 128*(2), 223–228.
- Brolin, K. (2002). *Cervical spine injuries-numerical analyses and statistical survey* (Unpublished doctoral dissertation). Institutionen för flygteknik.
- Brolin, K., Halldin, P., & Leijonhufvud, I. (2005). The effect of muscle activation on neck response. *Traffic injury prevention, 6*(1), 67–76.
- Brolin, K., Hedenstierna, S., Halldin, P., Bass, C., & Alem, N. (2008). The importance of muscle tension on the outcome of impacts with a major vertical component. *International journal of crashworthiness, 13*(5), 487–498.
- Burkhart, T. A., Andrews, D. M., & Dunning, C. E. (2013). Finite element modeling mesh quality, energy balance and validation methods: A review with recommendations associated with the modeling of bone tissue. *Journal of biomechanics, 46*(9), 1477–1488.
- Carlsson, S., & Davidsson, J. (2011). Volunteer occupant kinematics during driver initiated and autonomous braking when driving in real traffic environments. In *Proceedings of the international conference on biomechanics of impact ircobi, krakow-poland*.
- Choi, H. Y., Sah, S. J., Lee, B., Cho, H. S., Kang, S. J., Mun, M. S., . . . Lee, J. (2005). Experimental and numerical studies of muscular activations of bracing occupant. In *19th esv conference, paper*.
- Commission, E.-E., et al. (2011). Roadmap to a single european transport area-towards a competitive and resource efficient transport system. *White Paper, Communication, 144*.

- Deng, Y.-C., & Goldsmith, W. (1987). Response of a human head/neck/upper-torso replica to dynamic loading—ii. analytical/numerical model. *Journal of biomechanics*, 20(5), 487–497.
- Ejima, S., Ito, D., Satou, F., Mikami, K., Ono, K., Kaneoka, K., & Shiina, I. (2012). Effects of pre-impact swerving/steering on physical motion of the volunteer in the low-speed side-impact sled test. In *Proceedings of the 2012 international research council on biomechanics injury conference* (pp. 12–14).
- Ejima, S., Ono, K., Holcombe, S., Kaneoka, K., & Fukushima, M. (2007). A study on occupant kinematics behaviour and muscle activities during pre-impact braking based on volunteer tests. In *Proceedings of ircobi (international research council on the biomechanics of injury) conference 2007, held maastricht, the netherlands, september 2007*.
- Ejima, S., Ono, K., Kaneoka, K., & Fukushima, M. (2005). Development and validation of the human neck muscle model under impact loading. In *Proceedings of the international research council on the biomechanics of injury conference* (Vol. 33, pp. 11p–11p).
- Ejima, S., Zama, Y., Satou, F., Holcombe, S., Ono, K., Kaneoka, K., & Shiina, I. (2008). Prediction of the physical motion of the human body based on muscle activity during pre-impact braking. In *Proceedings of the ircobi conference* (pp. 163–175).
- Eliasson, E., & Wass, J. (2015). *Industrialisation of a finite element active human body model for vehicle crash simulations* (Master's thesis). Chalmers University of Technology, Department of Applied Mechanics, Chalmers University of Technology, Göteborg, Sweden. (Diploma work, nr: 2015:52)
- Energy, E. (2012). Transport in figures, 2012. *Office for Official Publications of the European Communities, Luxembourg*.
- Halldin, P. (2001). Prevention and prediction of head and neck injury in traffic accidents—using experimental and numerical methods.
- Hault-Dubrulle, A., Robache, F., Pacaux, M.-P., & Morvan, H. (2011). Determination of pre-impact occupant postures and analysis of consequences on injury outcome. part i: A driving simulator study. *Accident Analysis & Prevention*, 43(1), 66–74.
- Hill, A. (1938). The heat of shortening and the dynamic constants of muscle. *Proceedings of the Royal Society of London B: Biological Sciences*, 126(843), 136–195.
- Huber, P., Kirschbichler, S., Prügler, A., & Steidl, T. (2014). Three-dimensional occupant kinematics during frontal, lateral and combined emergency maneuvers. In *International ircobi conference on the biomechanics of impact, berlin, germany* (p. 668 - 669). Berlin, Germany.
- Huber, P., Kirschbichler, S., Prügler, A., & Steidl, T. (2015). Passenger kinematics in braking, lane change and oblique driving maneuvers. In *Proc. of ircobi* (p. 783 - 802). Lyon, France.
- Itskov, M. (2016). *Mechanics of living tissues*. RWTH Aachen University.
- Iwamoto, M., Kisanuki, Y., Watanabe, I., Furusu, K., Miki, K., & Hasegawa, J. (2002). Development of a finite element model of the total human model for safety (thumbs) and application to injury reconstruction. *Proceedings of*

- the 2002 International Research Council on Biomechanics of Injury, Munich, Germany*, 31–42.
- Iwamoto, M., Nakahira, Y., & Sugiyama, T. (2011). Investigation of pre-impact bracing effects for injury outcome using an active human fe model with 3d geometry of muscles. In *Proceedings of the 22nd esv conference* (pp. 11–0150).
- Jost, R., & Nurick, G. N. (2000). Development of a finite element model of the human neck subjected to high g-level lateral deceleration. *International journal of crashworthiness*, 5(3), 259–270.
- Kemper, A., Beeman, S., & Duma, S. (2011). Effects of pre-impact bracing on chest compression of human occupants in low-speed frontal sled tests. *SAE Journal*, 11, 1–6.
- Kirschbichler, S., Huber, P., Prügler, A., Steidl, T., Sinz, W., Mayer, C., & DAdetta, G. A. (2014). Factors influencing occupant kinematics during braking and lane change maneuvers in a passenger vehicle. In *International ircobi conference on the biomechanics of impact, berlin, germany*.
- Lie, A., Tingvall, C., Krafft, M., & Kullgren, A. (2006). The effectiveness of electronic stability control (esc) in reducing real life crashes and injuries. *Traffic injury prevention*, 7(1), 38–43.
- Maeno, T., & Hasegawa, J. (2001). Development of a finite element model of the total human model for safety (thums) and application to car-pedestrian impacts. In *Proceedings of 17th international esv conference* (pp. 1–10).
- Magnusson, M., Pope, M., Hasselquist, L., Bolte, K., Ross, M., Goel, V., . . . Wilder, D. (1999). Cervical electromyographic activity during low-speed rear impact. *European spine journal*, 8(2), 118–125.
- McHenry, R. R. (1963). Analysis of the dynamics of automobile passenger-restraint systems. In *Proceedings: American association for automotive medicine annual conference* (Vol. 7, pp. 207–249).
- Meijer, R., Rodarius, C., Adamec, J., van Nunen, E., & Van Rooij, L. (2008). A first step in computer modelling of the active human response in a far-side impact. *International journal of crashworthiness*, 13(6), 643–652.
- Meijer, R., Van Hassel, E., Broos, J., Elrofai, H., Van Rooij, L., & Van Hooijdonk, P. (2012). Development of a multi-body human model that predicts active and passive human behaviour. In *Proceedings of the international conference on biomechanics of impact ircobi, dublin-ireland* (pp. 622–636).
- Nemirovsky, N., & Van Rooij, L. (2010). A new methodology for biofidelic head-neck postural control. In *Proceedings of the international conference on biomechanics of impact ircobi, hannover-germany* (pp. 71–84).
- Norin, H., Carlsson, G., & Korner, J. (1984). *Seat belt usage in sweden and its injury reducing effect* (Tech. Rep.). SAE Technical Paper.
- Ólafsdóttir, J. M. (2017). *Muscle responses in dynamic events. volunteer experiments and numerical modelling for the advancement of human body models for vehicle safety assessment* (Doctoral dissertation). Division of Vehicle Safety, Department of Mechanics and Maritime Sciences, Chalmers University of Technology, Gothenburg. (Doctoral dissertation nr: 4275, ISBN=978-91-7597-594-8)
- Ólafsdóttir, J. M., Brodin, K., Blouin, J.-S., & Siegmund, G. P. (2015). Dynamic spatial tuning of cervical muscle reflexes to multidirectional seated perturbations.

- Spine*, 40(4), E211–E219.
- Ólafsdóttir, J. M., Östh, J., Davidsson, J., & Brodin, K. (2013). Passenger kinematics and muscle responses in autonomous braking events with standard and reversible pre-tensioned restraints. In *Ircobi conference 2013* (pp. 602–617).
- Östh, J. (2014). *Muscle responses of car occupants: Numerical modeling and volunteer experiments under pre-crash braking conditions* (Doctoral dissertation). Department of Applied Mechanics, Chalmers University of Technology, Gothenburg. (Doctoral dissertation nr: 3668, ISBN=978-91-7385-987-5)
- Östh, J., Ólafsdóttir, J. M., Davidsson, J., & Brodin, K. (2013). Driver kinematic and muscle responses in braking events with standard and reversible pre-tensioned restraints: validation data for human models. *Stapp car crash journal*, 57, 1.
- Östmann, M., & Jakobsson, L. (2016). An examination of pre-crash braking influence on occupant crash response using an active human body model. In *Ircobi conference proceedings*.
- Park, G., Kim, T., Crandall, J. R., Arregui Dalmases, C., & Narro, L. (2013). Comparison of kinematics of ghbm to pmhs on the side impact condition. In *2013 ircobi conference proceedings* (pp. 368–379).
- Penning, L. (1992). Acceleration injury of the cervical spine by hypertranslation of the head. *European Spine Journal*, 1(1), 13–19.
- Prasad, P., & Chou, C. C. (1993). A review of mathematical occupant simulation models. In *Accidental injury* (pp. 102–150). Springer.
- Prasad, P., & Chou, C. C. (2002). A review of mathematical occupant simulation models. In *Accidental injury* (pp. 121–186). Springer.
- Road Vehicles—Objective Rating Metric for Non-Ambiguous Signals* (Vol. 2014; Standard). (2014, August). Geneva, CH: International Organization for Standardization.
- Robin, S. (2001). Humos: human model for safety—a joint effort towards the development of refined human-like car occupant models. In *17th international technical conference on the enhanced safety vehicle* (p. 297).
- Scott, M. W., McConnell, W. E., Guzman, H. M., Howard, R. P., Bomar, J. B., Smith, H. L., ... Hatsell, C. P. (1993). *Comparison of human and atd head kinematics during low-speed rearend impacts* (Tech. Rep.). SAE Technical Paper.
- Shaw, J. M., Herriott, R. G., McFadden, J. D., Donnelly, B. R., & Bolte IV, J. H. (2006). Oblique and lateral impact response of the pmhs thorax. *Stapp car crash journal*, 50, 147.
- Shugar, T. A., & Katona, M. G. (1975). Development of finite element head injury model. *Journal of the Engineering Mechanics Division*, 101(3), 223–239.
- Siebert, T., Rode, C., Herzog, W., Till, O., & Blickhan, R. (2008). Nonlinearities make a difference: comparison of two common hill-type models with real muscle. *Biological cybernetics*, 98(2), 133–143.
- Stockman, I., Bohman, K., Jakobsson, L., & Brodin, K. (2013). Kinematics of child volunteers and child anthropomorphic test devices during emergency braking events in real car environment. *Traffic injury prevention*, 14(1), 92–102.
- van Rooij, L., Elrofai, H., Philippens, M., & Daanen, H. (2013). Volunteer kinematics and reaction in lateral emergency maneuver tests. *Stapp car crash journal*,

57, 313.

Yang, K. H., Hu, J., White, N. A., King, A. I., et al. (2006). Development of numerical models for injury biomechanics research: a review of 50 years of publications in the stapp car crash conference. *Stapp car crash journal*, 50, 429.

A

Code

A.1 Plot Kinematics with Corridor in MatLab

This MatLab code is intended to plot the kinematics of SAFER A-HBM with experimental corridor at load case brake. Code for plotting kinematics in load case lane change right and combined change right can be easily implemented by modifying this one. The coordinates of nodes in table 3.2 need to be saved as .csv files from LS-PrePost.

```
%%
clear all
close all
clc

%% Import data from text file.
my matlab folder = pwd
cd 'C:\YOURPATH_for_testing_data'

folders={'Brake50_01'};
j=1;
for k=1:size(folders,1)
    cd(folders{k})
    files=dir;
    files={files.name}';
    for i=3:(size(files,1))
        if strcmp(files{i}(end-2:end),'dat')
            if ~strncmpi(files{i},'~',1)
                %% Choose output
                output_index=22;

                % 1 t s
                % 2 BeltForceUpper kN
                % 3 BeltForceLower kN
                % 4 SteeringWheelAngle deg
                % 5 SteeringWheelAngularVelocity deg/s
                % 6 Velocity km/s
                % 7 YawRate deg/s
                % 8 AccelerationX m s^-2
                % 9 AccelerationY m s^-2
                % 10 AngleHeadX deg phi_head_x
                % 11 AngleHeadY deg
                % 12 AngleHeadZ deg
                % 13 AngleTorsoX deg phi_torso_x
            end
        end
    end
end
```



```

        'VarName7', 'VarName8', 'VarName9', 'VarName10', ...
        'VarName11', 'VarName12', 'VarName13', 'VarName14', ...
        'VarName15', 'VarName16', 'VarName17', 'VarName18', ...
        'VarName19', 'VarName20', 'VarName21', 'VarName22', ...
        'VarName23', 'VarName24', 'VarName25', 'VarName26', ...
        'VarName27', 'VarName28', 'VarName29', 'VarName30', ...
        'VarName31', 'VarName32', 'VarName33'});

    %% Clear temporary variables
    clearvars filename delimiter startRow formatSpec fileID ...
        dataArray ans;

    %% Check if the file has 331 data points
    data_points=height(tempoutput(:,1));
    if (data_points==331)
        output(:,j) = tempoutput{1:331,outputput_index};
        time(:,j) = tempoutput{1:331,1};
    else
        file_num_index=i-2;
        fprintf('The file: %s \n',files{i});
fprintf('has only %d data point, not 331, this subject is discarded \n',...
        data_points);
        j=j-1;
    end
    end
    end
    end
    j=j+1;
end
end

%% Create a matrix and compute the mean of each row for all subjects
output_avr=mean(output,2);

%% Compute the median of each row for all subjects
% If A is a matrix, then median(A,2) is a column vector containing the
% median value of each row.
output_median=median(output,2);

%% Compute the 0.16th and 0.84th quantile of each row for all subjects
output_16th=quantile(output,0.16,2);
output_84th=quantile(output,0.84,2);

%% Used when plot -PHI-phi
% figure('Position', [100, 100, 1049, 895])

figure('Position', [100, 100, 849, 695]);clf;hold on
plot(time(:,1),output_median,'—', 'color', [0.5 0.5 0.5],'linewidth',2);
plot(time(:,1),output_16th,'—', 'color', [0.5 0.5 0.5],'linewidth',2);
plot(time(:,1),output_84th,'—', 'color', [0.5 0.5 0.5],'linewidth',2);

%%
fprintf('\n outputput_index = %d \n\n',outputput_index);

myfolders={'D:\simulations\YOURPATH for SAFER A-HBM\RESULTS',...
'D:\simulations\YOURPATH for Passive HBM\RESULTS',...
'D:\simulations\YOURPATH for Taurus Seat\RESULTS',...

```

A. Code

```
        'D:\simulations\YOURPATH for No Pedal\RESULTS'...
    }';

% Used as counting for plotting figure of -PHI-phi.
yang2 = 0;

% Print on command window about where are simulations from
for yang0=1:size(myfolders,1)
    fprintf('Simulations are from: %s \n',myfolders{yang0});
end

% Go through all the folders in "myfolders"
for yang=1:length(myfolders)

    cd(myfolders{yang});

    files=dir;
    files={files.name}';

    l = 1; % Count the columns that have been read

    ifbeltforce=0; % Distinguish the data from belt force or kinematics

    for i=3:(size(files,1))
        if strcmp(files{i}(end-2:end),'csv')
            if ~strncmpi(files{i},'~',1)
                if ~strcmp(files{i},'beltforce.csv')
                    temp = xlsread(files{i});
                    tempFH(:,1) = temp(3:length(temp),2);
                    l = l+1;
                else
                    temp2 = xlsread(files{i});
                    tempbeltforce = temp2(3:length(temp2),:);
                    ifbeltforce=1;
                end
            end
        end
    end
    t=temp(3:length(temp),1);
    t=t/1000; % Time in data files is in ms
    if ifbeltforce==1
        t_bf=temp2(3:length(temp2),1);
        t_bf=t_bf/1000;
    end

    if ~(l==22) % Check if data are from all 21 files or some of them
        fprintf('\n ===== WARNING!! ===== \n');
    fprintf('Not having 21 files for femoral head, only input %d files\n'...
        ,l);
    end

    %% Read the data for belt force
    if ifbeltforce==1
        upbeltfoce=[];
        downbeltfoce=[];
        for i=1:length(tempbeltforce(:,1))
```

```

        upbeltfoce(i,1)=1/3*(tempbeltforce(i,14)+tempbeltforce(i,16)+...
            tempbeltforce(i,18));
        downbeltfoce(i,1) = 1/2*(1/3*(tempbeltforce(i,2) + ...
            tempbeltforce(i,4) + tempbeltforce(i,6))+...
            1/3*(tempbeltforce(i,8) + tempbeltforce(i,10) + ...
            tempbeltforce(i,12)));
    end
end

%% Read the data for kinematics
RFH=zeros(length(tempFH(:,1)),3);
LFH=zeros(length(tempFH(:,1)),3);
HeadTOP = zeros(length(tempFH(:,1)),3);
T5_sternum = zeros(length(tempFH(:,1)),3);
T1 = zeros(length(tempFH(:,1)),3);
T5 = zeros(length(tempFH(:,1)),3);
HeadCOG = zeros(length(tempFH(:,1)),3);
H_point=zeros(length(tempFH(:,1)),3);
torso_c=zeros(length(tempFH(:,1)),3);
r_torso=zeros(length(tempFH(:,1)),3);
torso_c_T1_vec=zeros(length(tempFH(:,1)),3);
torso_c_HeadCOG_vec = zeros(length(tempFH(:,1)),3);
r_head = zeros(length(tempFH(:,1)),3);
HeadCOG_HeadTOP_vec = zeros(length(tempFH(:,1)),3);
for l=1:3
    HeadCOG(:,l) = tempFH(:,l);
    RFH(:,l)=tempFH(:,3+l);
    LFH(:,l)=tempFH(:,6+l);
    HeadTOP(:,l) = tempFH(:,9+l);
    T5_sternum(:,l) = tempFH(:,12+l);
    T1(:,l) = tempFH(:,15+l);
    T5(:,l) = tempFH(:,18+l);
end

% Calculate kinematics parameters based on coordinates of nodes
for i=1:length(LFH(:,1))
    for j=1:3
        H_point(i,j) = 0.5*(RFH(i,j) + LFH(i,j));
        torso_c(i,j) = 3*T5(i,j)/3 + 0*T5_sternum(i,j)/3 ;
        torso_c_T1_vec(i,j) = T1(i,j) - torso_c(i,j);
        HeadCOG_HeadTOP_vec(i,j) = HeadTOP(i,j)-HeadCOG(i,j);
        r_torso(i,j) = torso_c(i,j) - H_point(i,j);
        r_head(i,j) = HeadCOG(i,j) - H_point(i,j);
    end
end
for i=1:length(torso_c(:,1))
    for j=1:3
        dr_torso(i,j)= r_torso(i,j) - r_torso(50,j);
        % The no. 50 is 241 ms and get (0,0) at 241 ms
        dr_head(i,j) = r_head(i,j) - r_head(50,j);
        dr_torso(i,j)= dr_torso(i,j)*(-1);\label{AppA1_1}
        % Due 2 the simulation & the car have opposite x to each other
        dr_head(i,j) = dr_head(i,j)*(-1);
    end
end
end

```

```
temp =[];
tempFH =[];

%% To caculate the PHI_torso_y
for i=1:length(r_torso(:,1))
    a = r_torso(50,:);
    b = r_torso(i,:);
    r = vrrotvec(a, b);
    PHI_torso_y(i) = 180 * (r(2)*r(4)) / pi;
end
%% To caculate the phi_torso_y
for i=1:length(torso_c_Tl_vec(:,1))
    a = torso_c_Tl_vec(50,:);
    b = torso_c_Tl_vec(i,:);
    r = vrrotvec(a, b);
    phi_torso_y(i) = 180 * (r(2)*r(4)) * (-1) / pi;
end

%% Output the r and phi
if (outputput_index<0)
    fprintf('\n ===== WARNING!! ===== \n');
    fprintf('outputput_index < 0 \n');
elseif (outputput_index==12)
    %% To caculate the phi_head_z
    for i=1:length(HeadCOG_HeadTOP_vec(:,1))
        a = HeadCOG_HeadTOP_vec(50,:);
        b = HeadCOG_HeadTOP_vec(i,:);
        r = vrrotvec(a, b);
        phi_head_z(i) = 180 * (r(3)*r(4)) * (+1) / pi;
        % The same movement goes to same z .
        % Car: head goes z posi
        % Simulation: head goes z posi
    end
    phi_head_z = phi_head_z';
    size(phi_head_z);
    size(t);
    plot(t-0.241,phi_head_z,'-','linewidth',2);
    h=legend(' Median ', 'quantile $16^{th}$', 'quantile $84^{th}$',...
            'AHBM', 'Passive AHBM', 'Taurus Seat', 'No pedal');
    set(h, 'interpreter', 'latex', 'fontsize', 20)
    xlabel('t(s)', 'fontsize', 20)
    set(ylabel('$\phi ^{Head}_{z}$'), 'interpreter', 'latex', ...
        'fontsize', 20)
    set(gca, 'fontsize', 25)
    axis([-0.30 1.5 -15 15])
    grid on
elseif (outputput_index==13)
    %% To caculate the phi_torso_x
    for i=1:length(torso_c_Tl_vec(:,1))
        a = torso_c_Tl_vec(50,:);
        b = torso_c_Tl_vec(i,:);
        r = vrrotvec(a, b);
        phi_torso_x(i) = 180 * (r(1)*r(4)) * (-1) / pi;
```

```

end
plot(t-0.241,phi_torso_x,'--','linewidth',1.5);
h=legend(' Median ','quantile $16^{th}$','quantile $84^{th}$',...
        'Passive HBM');
set(h,'interpreter','latex','fontsize',20)
xlabel('t(s)','fontsize',20)
set(ylabel('$\phi ^{Torso}_x$'),'interpreter','latex',...
    'fontsize',20)
set(gca,'fontsize',25)
axis([-0.30 1.6 -20 10])
grid on

elseif (outputput_index==14)
    %% To caculate the phi_torso_y
    for i=1:length(torso_c_Tl_vec(:,1))
        a = torso_c_Tl_vec(50,:);
        b = torso_c_Tl_vec(i,:);
        r = vrrotvec(a, b);
        phi_torso_y(i) = 180 * (r(2)*r(4)) * (-1) / pi;
    end
    plot(t-0.241,phi_torso_y,'-', 'linewidth',2);
    h=legend(' Median ','quantile $16^{th}$','quantile $84^{th}$',...
            'AHBM','Passive AHBM');
    set(h,'interpreter','latex','fontsize',20)
    xlabel('t(s)','fontsize',20)
    set(ylabel('$\phi ^{Torso}_y$'),'interpreter','latex',...
        'fontsize',20)
    set(gca,'fontsize',25)
    axis([-0.30 1.0 -30 25])
    grid on

elseif (outputput_index==15)
    %% To caculate the phi_torso_z
    for i=1:length(torso_c_Tl_vec(:,1))
        a = torso_c_Tl_vec(50,:);
        b = torso_c_Tl_vec(i,:);
        r = vrrotvec(a, b);
        phi_torso_z(i) = 180 * (r(3)*r(4)) * (+1) / pi;
    end
    phi_torso_z = phi_torso_z';
    size(phi_torso_z);
    size(t);
    plot(t-0.241,phi_torso_z,'-', 'linewidth',2);
    h=legend(' Median ','quantile $16^{th}$','quantile $84^{th}$',...
            'AHBM','Passive AHBM','Taurus Seat','No pedal');
    set(h,'interpreter','latex','fontsize',20)
    xlabel('t(s)','fontsize',20)
    set(ylabel('$\Delta r^{Head}_y$'),'interpreter','latex',...
        'fontsize',20)
    set(gca,'fontsize',25)
    axis([-0.30 1.5 -15 15])
    grid on

elseif (outputput_index==22)
    %% dr_head_x
    plot(t-0.241,dr_head(:,1),'-', 'linewidth',2);

```

```
h=legend(' Median ', 'quantile $16^{th}$', 'quantile $84^{th}$', ...
        'AHBM', 'Passive AHBM', 'Taurus Seat');
set(h, 'interpreter', 'latex', 'fontsize', 20)
xlabel('t(s)', 'fontsize', 20)
set(ylabel('$\Delta r^{Head}_{y}$'), 'interpreter', 'latex', ...
    'fontsize', 20)
set(gca, 'fontsize', 25)
axis([-0.30 1.3 -265 30])
grid on

elseif (outputput_index==23)
    %% dr_head_y
    plot(t-0.241, dr_head(:,2), '-', 'linewidth', 2);

    h=legend(' Median ', 'quantile $16^{th}$', 'quantile $84^{th}$', ...
            'AHBM', 'Passive AHBM', 'Taurus Seat');
    set(h, 'interpreter', 'latex', 'fontsize', 20)
    xlabel('t(s)', 'fontsize', 20)
    set(ylabel('$\Delta r^{Head}_{y}$'), 'interpreter', 'latex', ...
        'fontsize', 20)
    set(gca, 'fontsize', 25)
    axis([-0.50 2.5 -300 300])
    grid on

elseif (outputput_index==25)
    %% dr_torso_x
    plot(t-0.241 , dr_torso(:,1) , '-', 'linewidth', 2);

    h=legend(' Median ', 'quantile $16^{th}$', 'quantile $84^{th}$', ...
            'AHBM', 'Passive AHBM', 'Taurus Seat');
    set(h, 'interpreter', 'latex', 'fontsize', 20)
    xlabel('t(s)', 'fontsize', 20)
    set(ylabel('$\Delta r^{Head}_{y}$'), 'interpreter', 'latex', ...
        'fontsize', 20)
    set(gca, 'fontsize', 25)
    axis([-0.30 1.3 -100 30])
    grid on

elseif (outputput_index==26)
    %% dr_torso_y
    plot(t-0.241, dr_torso(:,2), '-', 'linewidth', 2);

    h=legend(' Median ', 'quantile $16^{th}$', 'quantile $84^{th}$', ...
            'AHBM', 'Passive AHBM', 'Taurus Seat');
    set(h, 'interpreter', 'latex', 'fontsize', 20)
    xlabel('t(s)', 'fontsize', 20)
    set(ylabel('$\Delta r^{Head}_{y}$'), 'interpreter', 'latex', ...
        'fontsize', 20)
    set(gca, 'fontsize', 25)
    axis([-0.50 2.5 -300 300])
    grid on

%% Uncomment section when calculating the PHI - phi
% elseif (outputput_index==31)
```

```

%% To caculate the PHI_torso_x
for i=1:length(r_torso(:,1))
    a = r_torso(50,:);
    b = r_torso(i,:);
    r = vrrotvec(a, b);
    PHI_torso_x(i) = 180 * (r(1)*r(4)) / pi;
    % the same movement goes to different coordinate system.
    % car: head goes x nega, y posi
    % simu: head goes x posi, y negi
end
plot(t-0.241,PHI_torso_x,'-', 'linewidth',2);

h=legend(' Median ', 'quantile $16^{th}$', 'quantile $84^{th}$', ...
        'AHBM', 'Passive AHBM', 'Taurus Seat');
set(h, 'interpreter', 'latex', 'fontsize',20)
xlabel('t (s)', 'fontsize',20)
set(ylabel('$\Delta r^{Head}_{y}$'), 'interpreter', 'latex', ...
    'fontsize',20)
set(gca, 'fontsize',25)
axis([-0.50 2.5 -60 55])
grid on
% % %

%% Uncomment section when calculating the PHI - phi
elseif (outputput_index==32)
    %% To caculate the PHI_torso_y
    for i=1:length(r_torso(:,1))
        a = r_torso(50,:);
        b = r_torso(i,:);
        r = vrrotvec(a, b);
        PHI_torso_y(i) = 180 * (r(2)*r(4)) / pi;
    end
    plot(t-0.241,PHI_torso_y,'-', 'linewidth',2);

    h=legend(' Median ', 'quantile $16^{th}$', 'quantile $84^{th}$', ...
            'AHBM', 'Passive AHBM', 'Taurus Seat');
    set(h, 'interpreter', 'latex', 'fontsize',20)
    xlabel('t (s)', 'fontsize',20)
    set(ylabel('$\Delta r^{Head}_{y}$'), 'interpreter', 'latex', ...
        'fontsize',20)
    set(gca, 'fontsize',25)
    axis([-0.30 1.6 -5 25])
    grid on
% % %

elseif (outputput_index==33)
    %% To caculate the PHI_torso_z
    plot(t-0.241,PHI_torso_z,'--', 'linewidth',2);

    h=legend(' Median ', 'quantile $16^{th}$', 'quantile $84^{th}$', ...
            'AHBM', 'Passive AHBM', 'Taurus Seat');
    set(h, 'interpreter', 'latex', 'fontsize',20)
    xlabel('t (s)', 'fontsize',20)
    set(ylabel('$\Delta r^{Head}_{y}$'), 'interpreter', 'latex', ...
        'fontsize',20)
    set(gca, 'fontsize',25)

```

A. Code

```
axis([-0.30 1.6 -20 10])
grid on

end

if (outputput_index==31)
    %% To caculate the -PHI_torso_x - phi_torso_x
    for i=1:length(r_torso(:,1))
        a = r_torso(50,:);
        b = r_torso(i,:);
        r = vrrotvec(a, b);
        PHI_torso_x(i) = 180 * (r(1)*r(4)) / pi;
        % the same movement goes to different coordinate system.
        % car: head goes x nega, y posi
        % simu: head goes x posi, y negi
    end

    for i=1:length(torso_c_T1_vec(:,1))
        a = torso_c_T1_vec(50,:);
        b = torso_c_T1_vec(i,:);
        r = vrrotvec(a, b);
        phi_torso_x(i) = 180 * (r(1)*r(4))*(-1) / pi;
    end
    dPHIphi_torso_x = -PHI_torso_x - phi_torso_x;
    if yang == 1
        figure('Position', [100, 100, 849, 695]);hold on
    end
    plot(t-0.241,dPHIphi_torso_x,'-', 'linewidth',2);

    h=legend(' Median ', 'quantile $16^{th}$', 'quantile $84^{th}$', ...
            'AHBM', 'Passive AHBM', 'Taurus Seat');
    set(h, 'interpreter', 'latex', 'fontsize',20)
    xlabel('t(s)', 'fontsize',20)
    set(ylabel('$-\Phi ^{Torso}_x-\phi ^{Torso}_x$'), ...
        'interpreter', 'latex', 'fontsize',20)
    set(gca, 'fontsize',25)
    axis([-0.50 2.5 -10 15])
    grid on

end

if (outputput_index==32)
    %% To caculate the -PHI_torso_y - phi_torso_y
    for i=1:length(r_torso(:,1))
        a = r_torso(50,:);
        b = r_torso(i,:);
        r = vrrotvec(a, b);
        PHI_torso_y(i) = 180 * (r(2)*r(4)) / pi;
        % The same movement goes to different coordinate system.
        % Car: head goes x nega, y posi
        % Simulation: head goes x posi, y negi
    end

    for i=1:length(torso_c_T1_vec(:,1))
        a = torso_c_T1_vec(50,:);
        b = torso_c_T1_vec(i,:);
        r = vrrotvec(a, b);
    end
end
```

```

        phi_torso_y(i) = 180 * (r(2)*r(4))*(-1) / pi;
    end
    cd(my matlab folder);

    load('PHI_torso_y_output.mat')
    load('smallphi_torso_y_output.mat')
    % For saving data as .mat file
    % output_16th = quantile(output,0.16,2);
    % output_median = median(output,2);
    dPHIphi_torso_y_graz_output = ...
        -PHI_torso_y_output - smallphi_torso_y_output;

    dPHIphi_torso_y_graz_output_median = ...
        median(dPHIphi_torso_y_graz_output,2);
    dPHIphi_torso_y_graz_output_16th = ...
        quantile(dPHIphi_torso_y_graz_output,0.16,2);
    dPHIphi_torso_y_graz_output_84th = ...
        quantile(dPHIphi_torso_y_graz_output,0.84,2);

    dPHIphi_torso_y = -PHI_torso_y - phi_torso_y;
%     For the first time of the loop, position plot of the corridor
%     figure('Position', [100, 100, 849, 695]);hold on

% If it is the first time of the loop, plot the corridor
if yang == 1
    plot(time(:,1),dPHIphi_torso_y_graz_output_median,'--',...
        'color', [0.5 0.5 0.5],'linewidth',2);
    plot(time(:,1),dPHIphi_torso_y_graz_output_16th,'--',...
        'color', [0.5 0.5 0.5],'linewidth',2);
    plot(time(:,1),dPHIphi_torso_y_graz_output_84th,'--',...
        'color', [0.5 0.5 0.5],'linewidth',2);
%     yang2 = 1;
end

plot(t-0.241,dPHIphi_torso_y,'-','linewidth',2);

h=legend(' Median ', 'quantile $16^{th}$', 'quantile $84^{th}$', ...
        'AHBM', 'Passive AHBM', 'Taurus Seat');
set(h, 'interpreter', 'latex', 'fontsize', 20)
xlabel('t (s)', 'fontsize', 20)
set(ylabel('$-\Phi ^{\text{Torso}}_y-\phi ^{\text{Torso}}_y$'), ...
    'interpreter', 'latex', 'fontsize', 20)
set(gca, 'fontsize', 25)
axis([-0.30 1.5 -15 15])
grid on

end

% Code that saves the median, 16th, and 84 th of PHI and phi as corridor
% Run these lines first when plot -PHI-phi
% %     figure('Position', [100, 100, 849, 695]);hold on %
% plot(time(:,1),-PHI_torso_y_output_median,'-', 'color', [0.5 0.5
% 0.5],'linewidth',2); %
% plot(time(:,1),-PHI_torso_y_output_16th,'-', 'color', [0.5 0.5
% 0.5],'linewidth',2); %
% plot(time(:,1),-PHI_torso_y_output_84th,'-', 'color', [0.5 0.5
% 0.5],'linewidth',2); %

```

A. Code

```
% plot(time(:,1),smallphi_torso_y_output_median,'--', 'color', [0.5 0.5
% 0.5], 'linewidth',2); %
% plot(time(:,1),smallphi_torso_y_output_16th,'--', 'color', [0.5 0.5
% 0.5], 'linewidth',2); %
% plot(time(:,1),smallphi_torso_y_output_84th,'--', 'color', [0.5 0.5
% 0.5], 'linewidth',2); % %
% plot(time(:,1),-PHI_torso_y_output_median -
% smallphi_torso_y_output_median,'-', 'linewidth',2); %
% plot(time(:,1),-PHI_torso_y_output_median -
% smallphi_torso_y_output_16th,'-', 'linewidth',2); %
% plot(time(:,1),-PHI_torso_y_output_median -
% smallphi_torso_y_output_84th,'-', 'linewidth',2); % If just substruct the
% corresponding edge, if two corridors are the same, then 3 lines are all
% 0. %           % should include every volunteer data, and redo the quantile
% 16 84.

% cd('Y:\Yang\MatLab_script\output_nodeXYZ\Passive_AHBM_Corridor_brake')
% PHI_torso_y_output_median = output_median; PHI_torso_y_output_16th =
% output_16th; PHI_torso_y_output_84th = output_84th;
% save('PHI_torso_y_output_median.mat', 'PHI_torso_y_output_median')
% save('PHI_torso_y_output_16th.mat', 'PHI_torso_y_output_16th')
% save('PHI_torso_y_output_84th.mat', 'PHI_torso_y_output_84th')
%
% cd('Y:\Yang\MatLab_script\output_nodeXYZ\Passive_AHBM_Corridor_brake')
% smallphi_torso_y_output_median = output_median;
% smallphi_torso_y_output_16th = output_16th;
% smallphi_torso_y_output_84th = output_84th;
% save('smallphi_torso_y_output_median.mat',...
% 'smallphi_torso_y_output_median')
% save('smallphi_torso_y_output_16th.mat', 'smallphi_torso_y_output_16th')
% save('smallphi_torso_y_output_84th.mat', 'smallphi_torso_y_output_84th')

% cd('Y:\Yang\MatLab_script\output_nodeXYZ\Passive_AHBM_Corridor_brake')
% % output_16th=quantile(output,0.16,2);
% PHI_torso_y_output = output;
% save('PHI_torso_y_output.mat', 'PHI_torso_y_output')

% cd('Y:\Yang\MatLab_script\output_nodeXYZ\Passive_AHBM_Corridor_brake')
% smallphi_torso_y_output = output;
% save('smallphi_torso_y_output.mat', 'smallphi_torso_y_output')

if (outputput_index==2)
    %% To caculate the BeltForceUpper    kN
    plot(t_bf-0.241,upbeltfoce,'-', 'linewidth',2);
    h=legend(' Median ', 'quantile $16^{th}$', 'quantile $84^{th}$', 'AHBM');
    set(h, 'interpreter', 'latex', 'fontsize',20)
    xlabel('t (s)', 'fontsize',20)
    set(ylabel('$ kN $'), 'interpreter', 'latex', 'fontsize',20)
    set(gca, 'fontsize',25)
    axis([-0.30 1. -0.1 0.3])
    grid on
```

```

end
if (output_index==3)
    %% To caculate the BeltForceDown    kN
    plot(t_bf-0.241,downbeltfoce,'-', 'linewidth',2);
    h=legend(' Median ', 'quantile $16^{th}$', 'quantile $84^{th}$', 'AHBM');
    set(h, 'interpreter', 'latex', 'fontsize',20)
    xlabel('t(s)', 'fontsize',20)
    set(ylabel('$ kN $'), 'interpreter', 'latex', 'fontsize',20)
    set(gca, 'fontsize',25)
    axis([-0.30 1. -0.1 0.3])
    grid on

end

% Reset the parameters, otherwise error occurring when you plot % more than one s
RFH=[];
LFH=[];
HeadTOP = [];
T5_sternum = [];
T1 = [];
T5 = [];
HeadCOG = [];
H_point=[];
torso_c=[];
r_torso=[];
torso_c_T1_vec=[];
torso_c_HeadCOG_vec = [];
r_head = [];
HeadCOG_HeadTOP_vec = [];
dr_torso=  [];
dr_head =  [];
dr_torso=  [];
dr_head =  [];
PHI_torso_x =  [];
PHI_torso_y =  [];
phi_torso_x =  [];
phi_torso_y =  [];
phi_torso_z =  [];
phi_head_z =  [];
end

```

A.2 Output Node Macro in LS-PrePost

After run this LS-PrePost macro command file, the X, Y, and Z coordinates would be output to .csv files separately for every node and every axis.

```
*lsprepost macro command file
*macro begin postnodeid
genselect target node
genselect node add node 8152925/0
ntime 1
xyplot 1 savefile ms_csv "YOUR_PATH\RESULTS\8152925_x_RFH.csv" 1 all
deletewin 1
ntime 2
xyplot 1 savefile ms_csv "YOUR_PATH\RESULTS\8152925_y_RFH.csv" 1 all
deletewin 1
ntime 3
xyplot 1 savefile ms_csv "YOUR_PATH\RESULTS\8152925_z_RFH.csv" 1 all
deletewin 1
clearpick
genselect node add node 8252925/0
ntime 1
xyplot 1 savefile ms_csv "YOUR_PATH\RESULTS\8252925_x_LFH.csv" 1 all
deletewin 1
ntime 2
xyplot 1 savefile ms_csv "YOUR_PATH\RESULTS\8252925_y_LFH.csv" 1 all
deletewin 1
ntime 3
xyplot 1 savefile ms_csv "YOUR_PATH\RESULTS\8252925_z_LFH.csv" 1 all
deletewin 1
clearpick
genselect node add node 8885602/0
ntime 1
xyplot 1 savefile ms_csv "YOUR_PATH\RESULTS\8885602_x_HeadTOP.csv" 1 all
deletewin 1
ntime 2
xyplot 1 savefile ms_csv "YOUR_PATH\RESULTS\8885602_y_HeadTOP.csv" 1 all
deletewin 1
ntime 3
xyplot 1 savefile ms_csv "YOUR_PATH\RESULTS\8885602_z_HeadTOP.csv" 1 all
deletewin 1
clearpick
genselect node add node 8925066/0
ntime 1
xyplot 1 savefile ms_csv "YOUR_PATH\RESULTS\8925066_x_STERNUM.csv" 1 all
deletewin 1
ntime 2
xyplot 1 savefile ms_csv "YOUR_PATH\RESULTS\8925066_y_STERNUM.csv" 1 all
deletewin 1
ntime 3
xyplot 1 savefile ms_csv "YOUR_PATH\RESULTS\8925066_z_STERNUM.csv" 1 all
deletewin 1
clearpick
genselect node add node 8990011/0
ntime 1
```

```
xyplot 1 savefile ms_csv "YOUR_PATH\RESULTS\8990011_x_T1.csv" 1 all
deletewin 1
ntime 2
xyplot 1 savefile ms_csv "YOUR_PATH\RESULTS\8990011_y_T1.csv" 1 all
deletewin 1
ntime 3
xyplot 1 savefile ms_csv "YOUR_PATH\RESULTS\8990011_z_T1.csv" 1 all
deletewin 1
clearpick
genselect node add node 8990051/0
ntime 1
xyplot 1 savefile ms_csv "YOUR_PATH\RESULTS\8990051_x_T5.csv" 1 all
deletewin 1
ntime 2
xyplot 1 savefile ms_csv "YOUR_PATH\RESULTS\8990051_y_T5.csv" 1 all
deletewin 1
ntime 3
xyplot 1 savefile ms_csv "YOUR_PATH\RESULTS\8990051_z_T5.csv" 1 all
deletewin 1
clearpick
genselect node add node 43700101/0
ntime 1
xyplot 1 savefile ms_csv "YOUR_PATH\RESULTS\43700101_x_HeadCOG.csv" 1 all
deletewin 1
ntime 2
xyplot 1 savefile ms_csv "YOUR_PATH\RESULTS\43700101_y_HeadCOG.csv" 1 all
deletewin 1
ntime 3
xyplot 1 savefile ms_csv "YOUR_PATH\RESULTS\43700101_z_HeadCOG.csv" 1 all
deletewin 1
clearpick
*macro end
```


B

Load Scenarios

The three load scenarios shown in the following figures were based on the data presented in Huber et al. (2015). The curves of brake event, lane change right event, and combined change right event scenarios were shown respectively in Figure B.1, Figure B.2, and Figure B.3. The positive longitudinal acceleration were the driving direction. The positive side acceleration was to the left of the driver.

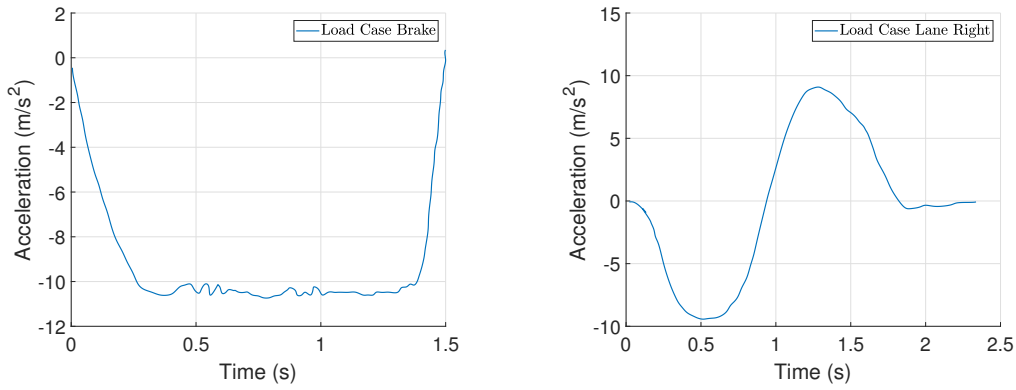


Figure B.1: Load Case Brake. Data is from Huber et al. (2015) **Figure B.2:** Load Case Lane Change Right. Data is from Huber et al. (2015)

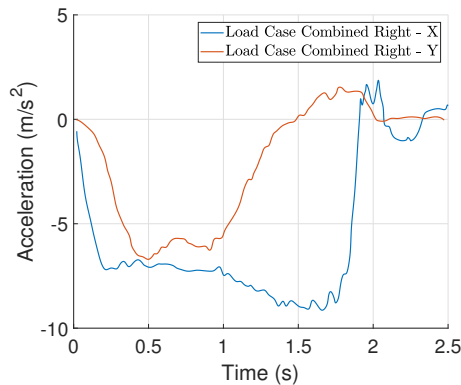


Figure B.3: Load Case Combined Change Right. Data is from Huber et al. (2015)